The Sediment Budget Estimator (SBE): a process-model for the stochastic estimation of fluxes and budgets of sediment through submarine channel systems.

Eggenhuisen, J.T.[1*], Tilston, M.C.[2], Stevenson, C.J.[3], Hubbard, S.M.[2], Cartigny, M.J.B.[4], Heijnen, M.S.[5], de Leeuw, J.[1], Pohl, F.[6], and Spychala, Y.T.[7]

*corresponding author: j.t.eggenhuisen@uu.nl

[1]Faculty of Geosciences, Utrecht University, the Netherlands.

[2]Department of Geoscience, University of Calgary, Canada.

[3]School of Environmental Sciences, University of Liverpool, United Kingdom.

[4]Departments of Earth Science and Geography, Durham University, United Kingdom.

[5]Ocean and Earth Science, University of Southampton, United Kingdom.

[6]School of Biological and Marine Sciences, University of Plymouth, United Kingdom.

[7]Institute of Geology, Leibniz University Hannover, Germany.

ABSTRACT

Turbidity currents transport vast amounts of sediment through submarine channels onto deep-marine basin floor fans. There is a lack of quantitative tools for the reconstruction of the sediment budget of these systems. The aim of this paper is to construct a simple and user-friendly model that can estimate turbidity-current structure and sediment budget based on observable submarine channel dimensions and general characteristics of the system of interest. The requirements for the model were defined in the spirit of the source-to-sink perspective of sediment volume modeling: a simple, quantitative model that reflects natural variability and can be applied to ancient systems with sparse data-availability. The model uses the input conditions to parameterize analytical formulations for the velocity and concentration profiles of turbidity currents. Channel cross-section and temporal punctuation of turbidity-current activity in the channel are used to estimate sediment flux and sediment budget. The inherent uncertainties of geological sediment budget estimations motivate a stochastic approach, which results in histograms of sediment budget estimations, rather than discrete values. The model is validated against small-scale experimental turbidity currents and the 1929 Grand Banks turbidity current. It is found to perform within acceptable margins of error for sediment flux predictions at these smallest and largest scales of turbidity currents possible on Earth. This success motivates application of the model to a reconstruction of the sediment budget related to Cretaceous slope-channel deposits (Tres Pasos Formation, Chile). The results give insight into the likely highly stratified concentration profile and the flow velocity of the Cretaceous turbidity currents that formed the deposits. They also yield estimates of the typical volume of sediment transported through the channels while they were active. These volumes are demonstrated to vary greatly depending on the geologic interpretation of the relation between observable deposit geometries and the dimensions of the flows that formed them. Finally, the shape of the probability density functions of predicted sediment budgets is shown to depend on the geological (un)certainty ranges. Correct geological interpretations of deep marine deposits are therefore indispensable for quantifications of sediment budgets in deep marine systems.

INTRODUCTION

The rationale in studies about turbidity currents and their deposits often refers to submarine fans being the most voluminous sedimentary bodies on Earth (Middleton, 1993) and turbidity currents the most prolific transport agents on the planet (Talling *et al.*, 2012), yet no study has succeeded in presenting a process model that can be used to relate the turbidity currents responsible for the flux of sediment to the volumes of submarine fan deposits (Jobe *et al.*, 2018). The budget of sediment transported onto submarine fans is governed by geological mechanisms that operate on thousands to millions of years involving climate, tectonics, and sea level variations, and it is measured in cubic kilometers [km^3]. The flux of sediment in turbidity currents is governed by complex particle-fluid dynamics operating on milliseconds to hours, and it is measured in cubic meters per second [m^3/s]. This disparate spread in scales and types of controls makes calculation of geological sediment budgets from flow processes one of the big challenges in marine geosciences.

The source-to-sink approach to studying the entire geological chain of sediment production and transport has gained prominence in the past decade. It holistically tracks the budget of sediment from weathering of bedrock in mountainous or hilly catchment areas (the source), through the various depositional environments along the transport path, all the way to the terminal depositional sink in the deep oceans (Somme *et al.*, 2009a; Walsh *et al.*, 2016). A strength of the source-to-sink approach has been that it made the ultimate simplification of the process of sediment transport, while still yielding robust and informative answers to geological problems. Sediment is simply distributed from the source to the sink, and the various depositional sub-systems that are passed along the pathway (rivers, deltas, the continental shelf) act to extract a certain fraction of the available sediment budget (Paola & Martin, 2012). This success may be counterintuitive when observed parallel to the development of process-based modelling efforts that seek increasingly more detailed and complex treatments of the dynamics of sediment transport (Cantero *et al.*, 2011; Abd El-Gawad *et al.*, 2012; Basani *et al.*, 2014; Kneller *et al.*, 2016). Herein we explore how turbidity-current processes can be incorporated in a source-to-sink approach without decreasing its robustness and viability. Such incorporation of process-modelling into source-to-sink studies is one of four key areas for future advances called for by Walsh et al. (2016) in their review of the past, present, and future of the source-to-sink perspective. Geological uncertainties in source-to-sink analyses are commonly large, which means that boundary conditions for model simulations are defined as probable ranges, rather than specific, discrete, values. We argue that this necessitates application of stochastic process-modelling approaches to predictions of fluxes of sediment into deep water. Furthermore, a successful geological tool should be a simple, quantitative model that reflects natural variability and can be applied to ancient systems (Sømme and Martinsen, 2017).

The aim of this study is to construct a simple and user-friendly model that can estimate turbidity current parameters and sediment budgets based on observable submarine channel parameters. The result is the Sediment Budget Estimator (SBE), a process-based turbidity-current model that predicts sediment budget transferred through submarine channels from the continental slope to submarine fans over geological timescales.

Three geometrical geological inputs are required: Submarine channel dimension (depth and width), the size of the median and coarsest sediment particles present on the bed, and submarinechannel gradient. These can be derived from subsurface datasets such as reflection seismic data, core, or well-logs (Samuel *et al.*, 2003), from chosen outcrop analogues or architectural data-stores (Baas *et al.*, 2005; Cullis *et al.*, 2019), modern oceanographic analogues (Covault *et al.*, 2011; Prather *et al.*, 2016), or source-to-sink predictions based on system style (Helland-Hansen *et al.*, 2016). An additional estimation of the range of depth average sediment concentration needs to be supplied. Input can be constrained by narrow bounds of uncertainty where reliable data is available, or broad ranges of values where estimates are poorly constrained.

The SBE uses these input ranges to parametrize analytical formulations for the velocity and concentration profiles of turbidity currents that are typical of the chosen system geometries. These currents will be referred to as “characteristic turbidity currents” in this paper. The sediment flux is determined by multiplying the velocity and concentration profiles. The first type of output of the SBE are illustrative examples of the size, velocity, and concentration distribution of characteristic turbidity currents, and a histogram of sediment fluxes [m^3/s] transported through the channel cross sections. These histograms reflect the range of possible outcomes given the uncertainties in the input boundary conditions, and embody the stochastic character of the SBE.

Secondly, the SBE estimates the system-scale sediment budgets on geological timescale. To obtain these, the user can input turbidity current recurrence time (Pirmez & Imran, 2003; Clare *et al.*, 2014; Allin *et al.*, 2018; Jobe *et al.*, 2018; Stacey *et al.*, 2019), event duration (Pirmez & Imran, 2003; Xu, 2011; Cooper, 2013; Clarke, 2016; Azpiroz-Zabala *et al.*, 2017), and geological system activity (Pirmez *et al.*, 2012). These inputs can be based on the user's understanding of their particular system, or on default values for system styles suggested in literature. Output of this module is a histogram of sediment budgets [km^3] on geological timescale.

The essence of this approach of estimating sediment budgets is similar to the paleohydrologic "fulcrum approach" to fluvial sediment-budget estimation as proposed by (Holbrook & Wanas, 2014) and applied by (Lin & Bhattacharya, 2017; Sharma *et al.*, 2017). The fulcrum method perceives a fluvial channel cross section as the pivot between the sediment load received from the up-stream domain and transmitted to a downstream domain. It analyzes the relation between local channel-fill deposit architecture and this expected sediment throughput. In this paper we will describe this model-approach with special emphasis on the connection between flow structures of turbidity currents, their specific geological basin setting, and the geometry of of submarine channels. Due consideration will eb given to deep-marine concepts that can be used to constrain simulations. The model is then validated against the smallest and largest scales of sediment delivery into deep basins for which accurate dynamic data are available: laboratory scale turbidity currents (de Leeuw *et al.*, 2016, 2018a) and the 1929 Grand Banks turbidity current (Heezen & Ewing, 1952; Kuenen, 1952; Stevenson *et al.*, 2018). The model is then be applied to estimate the sediment budget associated with Cretaceous submarine channel deposits exposed in the Tres Pasos Formation in Southern Chile (Hubbard *et al.*, 2010, 2014; Macauley & Hubbard, 2013; Hubbard et al., *2020*). This application demonstrates the importance of geological models derived from stratigraphic observations for sediment budget estimations. The statistical uncertainties in sediment budget estimates on geologic time-scales can be decreased by narrowing the confidence bounds through strict scrutiny of the geologic record. Hence, the predictability of source-to-sink transfer of sediment to the terminal depositional sink in the deep oceans depends on the strength and confidence of geological models.

FORMULATION OF THE TURBIDITY CURRENT FLOW-STRUCTURE MODEL

The backbone of the SBE is formed by analytical formulations for vertical profiles of velocity, *u(z),* and concentration, *c(z)*, in turbidity currents (Fig. 1a). These are coupled by two closure equations that relate the velocity and concentration in the flow: 1) a sediment bypass condition that relates the bed shear stress to the basal sediment concentration (Eggenhuisen *et al.*, 2017); and 2) a conventional formulation that relates the average sediment concentration to the bed shear stress (Kneller, 2003; García, 2008). Three boundary conditions need to be set by the user to be able to solve the system of equations: Submarine channel dimension (depth and width), the size of the median and coarsest sediment particles present on the bed, and submarine slope gradient.

Velocity Profile

The velocity profile of turbidity currents has been recognized to display robust, recurring patterns (Plapp & Mitchell, 1960; Stacey & Bowen, 1988; Garcia & Parker, 1993; Altinakar *et al.*, 1996; Kneller *et al.*, 1999; Kneller & Buckee, 2000; Best *et al.*, 2001; Xu *et al.*, 2002; Gray *et al.*, 2005; Straub *et al.*, 2008; Islam & Imran, 2010; Sequeiros *et al.*, 2010a; Xu, 2011; Eggenhuisen & McCaffrey, 2012; Sequeiros, 2012; Cartigny *et al.*, 2013; Cooper, 2013; Pittaluga & Imran, 2014; Azpiroz-Zabala *et al.*, 2017a; Sequeiros *et al.*, 2018). This robustness of the shape of the velocity profile results from the simple essential structure of turbidity currents: the bottom boundary is assumed to be a turbulent, wall-bound, shear layer; and the upper boundary is a turbulent mixing layer between the turbidity current and the ambient fluid. The velocity model developed here is therefore formed by the addition of two velocity functions: the logarithmic law of the wall, and a plane-mixing-layer velocity function. Different approaches have been proposed for the effective superposition of these functions (Altinakar *et al.*, 1996; Kneller *et al.*, 1999).

We follow the approach of Kneller et al. (1999;) instead of Altinakar et al. (1996), by assuming a logarithmic velocity profile from the bed to the flow depth, and applying a mixing layer structure throughout the water column (Fig. 2). We deviate slightly from Kneller et al. (1999) who use the “interface” between sediment laden and clear water as the flow depth. This interface can be qualitatively observed instantaneously in turbidity currents, e.g. in pictures of experiments, but due to the multitude of turbulent mixing structures passing any one location over time it cannot be quantitatively defined in a time-averaged structure of a turbidity current, where the velocity and concentration asymptotically approach 0 with height (Garcia & Parker, 1989; Islam & Imran, 2010; Sequeiros *et al.*, 2010b; de Leeuw *et al.*, 2018a). Instead, we follow Hermidas et al. (2018) by defining the elevation $z=H$ as the center of mixing layer and top of the logarithmic profile (Fig. 2). This measure of flow depth is equated to levee height in our approach (Fig. 1B). This definition is a key aspect of the modelling strategy, and will be further justified below.

The velocity u [m/s] as a function of elevation above the bed z [m] is then:

$$u(z) = u_{\log}(z) - u_{PML}(z) \tag{1}$$

The logarithmic velocity function is:

$$\begin{aligned} u_{\log}(z) &= \frac{u^*}{\kappa}\ln\left(\frac{z}{z_0}\right)\Bigg|_{z_0 \le z \le H} \\ u_{\log}(z) &= \frac{u^*}{\kappa}\ln\left(\frac{H}{z_0}\right)\Bigg|_{z \ge H} \end{aligned} \tag{2}$$

Where u^* is the shear velocity [m/s], κ is von Karman’s constant [0.4], z is the bed-perpendicular coordinate, and z_0 is the elevation at which the turbulent velocity profile intersects 0 m/s (Van Rijn, 2011).

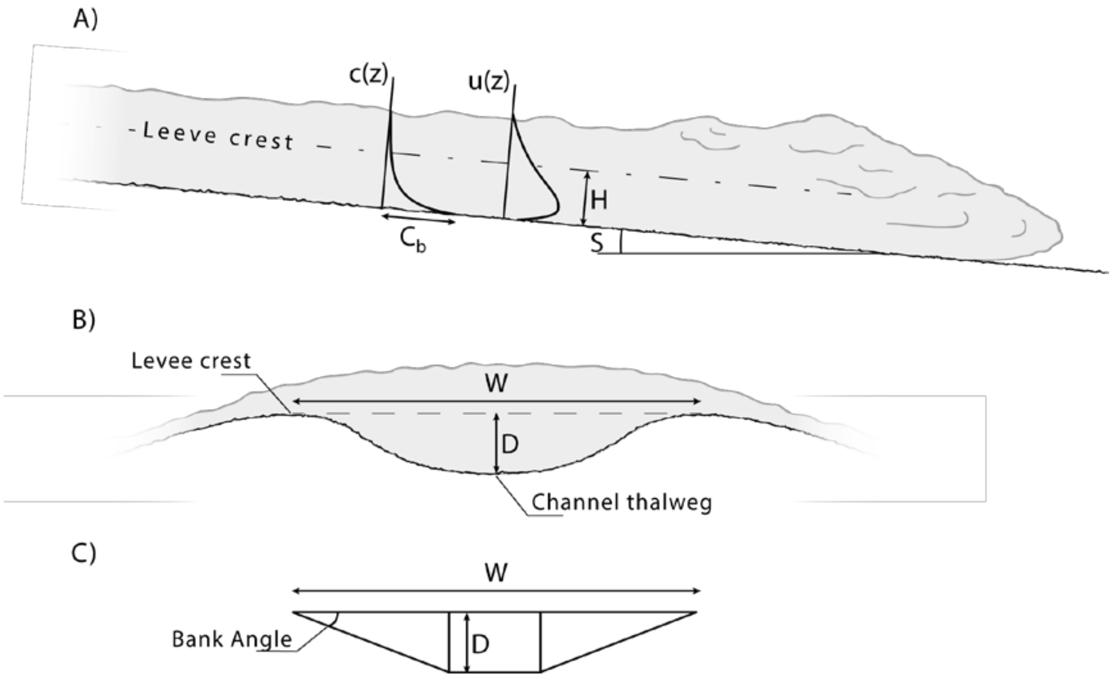

Fig. 1: *A) Schematic representation of the structure of a turbidity current, simplified from Altinakar et al. (1996). B) Schematic of the relation between channel cross-section and the modelled turbidity current. C) Trapezoidal cross-section of the model channel.*

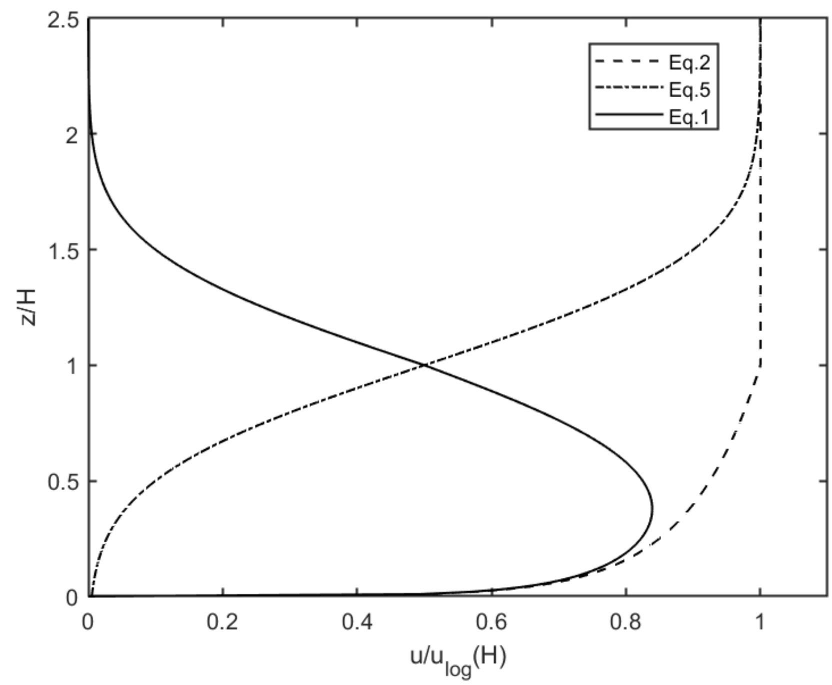

Fig. 2: *The analytical formulation for the velocity profile of turbidity currents (Eq. 1; solid line), as obtained by subtracting the PML term (Eq. 5; dash-dotted line) from the logarithmic velocity (Eq. 2; dashed line). Following Kneller et al. (1999) in lieu of Altinakar et al. (1996).*

The non-dimensional velocity distributions of plane mixing layers collapses into a universal function with the form (Champagne *et al.*, 1976; Pope, 2000):

$$f(\xi) = 1/2\, erf\left(\frac{\xi}{\sigma\sqrt{2}}\right) \tag{3}$$

Where σ has been analytically determined to be ~0.39 (Pope, 2000), and ξ is a non-dimensional coordinate perpendicular to the bed:

$$\xi = \left(z - z_{50}\right) / \left(z_{10} - z_{90}\right) \tag{4}$$

The subscripts denote the elevations of the velocity percentiles, e.g. z_{50} is the z-coordinate where the velocity is equal to 50% of the maximum velocity ($u_{log}(H)$). The range between z_{10} *and* z_{90} is approximated closely by *H* (Pope, 2000).

The scaled velocity function *f(ξ)* relates to the dimensional plane-mixing-layer velocity function as:

$$u_{PML}(\xi) = u_{\log}\left(H\right)\left[f(\xi) + 1/2\right] \tag{5}$$

Note that the plane mixing layer is scaled with the logarithmic velocity, not with the velocity maximum of the turbidity current (Kneller *et al.*, 1999). The maximum velocity, as well as the elevation of the maximum velocity of the turbidity current thus arise from the modelling, and are not constrained *a priori*. Equation 5 mathematically extends below the bed where it asymptotically approaches 0. The residual velocity of Eq. 5 at $z=0$ is 0.1% of $u_{log}(H)$, which is deemed insignificant for the purpose of modelling the sediment budget of submarine channel systems.

Concentration Profile

The shape of the concentration profile of many experiments is a rather similar, slightly concave exponential function (Garcia, 1994; Choux *et al.*, 2005; Islam & Imran, 2010; Sequeiros *et al.*, 2010a; Tilston *et al.*, 2015; de Leeuw *et al.*, 2018a). The concentration function is here expressed in the simplest form of an exponential decay function:

$$c(z) = C_b e^{-kz} \tag{6}$$

Where $c(z)$ is the sediment concentration at elevation z [m], C_b is the sediment concentration at the base of the flow [-], and k is a decay constant [1/m].

Closure Relations Between Variables

Sediment Bypass Closure --- Submarine channels are effective bypass conduits for sediment into deep basins (Stevenson *et al.*, 2015b; Kneller *et al.*, 2016) that remain open conduits for most of their lifespan (Hubbard *et al.*, 2014), such that the sediment mass eventually deposited in the channel-fill deposits at a given cross section represents only a minute portion of the sediment mass transported through that cross section (Paola & Martin, 2012; Stevenson *et al.*, 2015a; de Leeuw *et al.*, 2018b). A bypass condition is therefore used here to reconstruct the characteristic sediment flux going through a channel. The bypass condition is here based on the suspension capacity parameter Γ of Eggenhuisen et al. (2017), which balances the gravitational, buoyancy and turbulent forces acting on the suspended load. It includes universal turbulent flow scales and material properties of the fluid and particles only. The condition $\Gamma < 1$ coincides with the complete consumption of bed-generated turbulence by sediment suspension, as observed in direct numerical simulations (Cantero *et al.*, 2009, 2011, 2012). This over-saturated sediment condition is thought to lead to rapid deposition. The condition $\Gamma = 1$ can be used to relate the sediment concentration at the base of a bypassing turbidity current C_b to flow conditions and material properties of water and sediment (Eggenhuisen et al., 2017):

$$C_b = \frac{{u_*}^3}{140 \upsilon g R} \tag{7}$$

Where v [m^2/s] is the kinematic viscosity of water, g [m/s^2] is the acceleration by gravity, and R [-] is the submerged relative density of quartz in water (1.65).

Parameterization of the Logarithmic Velocity Profile --- Shear velocity and z_0 are the two parameters that are needed to resolve the logarithmic velocity function (Eq. 2).

The shear velocity is estimated from the shear stress at the base of the flow due the excess weight of suspended sediment:

$$u* = \sqrt{H_r \overline{C} gRS} \tag{8}$$

Where H_r is the hydraulic radius [m], which is calculated as the cross-sectional area divided by the frictional perimeter. The interface with the ambient fluid is included into the frictional perimeter here. $\overline{C}$ is the input depth-averaged sediment concentration [-], which is evaluated between the bed and *z=H (see Boundary Conditions, below). S* is the tangent of the slope [-].

Different empiric relations have been suggested for z_0 (Garcia, 2008; van Rijn, 2011). In the version used here, a distinction is made between mobile and non-mobile beds, based on the ratio between the bed shear stress (τ_b) and the critical bed shear stress (τ_c) for initiation of transport of the bed material ("transport stage" *sensu* van Rijn, 2011):

$$\begin{aligned} z_0 &= \frac{k_s}{30} + \frac{\nu}{9u^*}\bigg|_{\tau_b<\tau_c} \\ z_0 &= \frac{k_s}{30} + \delta_b\bigg|_{\tau_b\geq\tau_c} \end{aligned} \tag{9}$$

Where k_s is the Nikuradse equivalent sand roughness [m], and δ_b is the thickness of the bedload layer [m]. The Nikuradse equivalent sand roughness can be estimated from the grainsize of the coarsest sediment particles on the bed (d_{90}; 90th percentile of the grainsize distribution; van Rijn, 2011):

$$\begin{aligned} k_s &\approx 3d_{90}\left(sand\right) \\ k_s &\approx d_{90}\left(gravel\right) \end{aligned} \tag{10}$$

The thickness of the bedload layer is estimated as (Garcia, 2008):

$$\delta_b = \frac{0.015 d_{50}[\tau_b/\tau_c]}{1+0.2[\tau_b/\tau_c]}$$

Where d_{50} is the median grainsize of the bed material [m]. Form roughness effects related to irregular shapes of the bed (e.g. bedforms) are not incorporated in Eq. 9.

Boundary Conditions

The structure of equations 1-10 has been chosen such that they can now be solved when boundary condition values are set for flow thickness *H*, depth averaged sediment concentration $\overline{C}$, slope *S*, and characteristic bed-grainsize, which are all variables that deep marine geologists can estimate and debate. The probabilistic nature of the SBE will allow the users to rapidly test their ideas on the confidence bounds of these parameters. It is thus not necessary to know exactly how thick characteristic turbidity currents in a system of interest are, nor what their average concentration was. Rather, the model can be used to test the implications of perspectives on these parameters, perspectives that all deep marine geologists have, for predictions of sediment fluxes and budgets. This includes the perspective that it is wholly unknown what the scales of characteristic turbidity currents in a system are, as will be illustrated in the discussion. This probabilistic functionality is realized by requiring the user to define a range between likely minimum and maximum values for each of the boundary conditions. These ranges are uniformly sampled by the SBE with a user-defined number of steps in between the minimum and maximum values. Equations 1-10 are solved for all combinations of each of the boundary condition values. This can lead to thousands or tens of thousands turbidity currents being simulated.

Flow Thickness Correlates to Channel Depth --- Turbidity current thickness is often assumed to be closely related to the depth of the channel in modelling approaches (Salles *et al.*, 2009; Abd El-Gawad *et al.*, 2012; Arfaie *et al.*, 2014; Basani *et al.*, 2014; Hamilton *et al.*, 2017; Jobe *et al.*, 2017; Kane *et al.*, 2017). Such bank-full discharge assumptions are bread-and-butter in fluvial paleohydrology, but much less straightforward in channelized turbidity currents, which may extend above the channel. This key assumption of the model will therefore be addressed in depth. Firstly, the simple argument of scale is supported by the validity of laboratory modelling of channelized turbidity current morphodynamics (de Leeuw *et al.*, 2016), which demonstrates that laboratory-sized flows that are orders of magnitude smaller than real world flows self-generate channels at similar dimensions to the flows: small turbidity currents build small channels and large turbidity currents build large channels.

Furthermore, our morphodynamic understanding of levee-building includes a self-regulatory mechanism, whereby the levees aggrade by deposition from the dilute top of the flow, causing the levee-building to halt when the channel relief reaches a similar scale as the flow thickness (Straub & Mohrig, 2008; Shumaker et al., 2018)). Indeed, the variability of flow thickness with respect to channel dimensions has been argued to be small by Straub et al. (2008) who argue that the channel form and flow scale will always be tuned to each other. The robustness of this self-regulatory mechanism is reflected in the successful application of the geomorphological concept of hydraulic geometry (Leopold & Maddock, 1953) to submarine channels by Konsoer et al. (2013), who established that a correlative power-law relation between turbidity current discharge and submarine channel dimensions does exist.

Investigating the process of channelized flow in more detail, Mohrig and Buttles (2007) established experimentally that channels serve as effective conduits for turbidity currents that are 1.3 times thicker than the channel-form is deep. The along-axis flow velocities are an order of magnitude higher than the cross-channel overspill velocity in such confined flows. The ratio of along-axis to cross-channel velocity rapidly decreases for partially confined flows that are thicker than 1.3 times the channel depth (Mohrig & Buttles, 2007), indicating that those flows are poorly confined by the channel and rapidly spread out over the overbank area. Mohrig and Buttles (2007) use a conventional definition of flow thickness as the distance between the bed and an interface between ambient fluid and the turbidity current (H_{MB}). This interface is not defined in a time-averaged velocity profile, and falls somewhere in the top half of the mixing layer. The proposal of Hermidas et al. (2018) to define the center of the mixing layer as the flow depth (Fig. 2) is less ambiguous and more straightforward: the simple condition of $H=D$ (Fig. 1a&b) is roughly equal to the regime-boundary for fully channelized flows as defined by Mohrig and Buttles (2007), because $H_{MB}=1.3*D$, and $H=D$ here.

Finally, the bypass condition based on the suspension capacity parameter of Eggenhuisen et al. (2017) also contains a mechanism that causes channel dimensions to be attracted to a bypass state for the characteristic turbidity currents in the system. If the concentration at the base of the flow exceeds the saturation concentration, this will lead to the immediate deposition of excess sediment on the bed, until $\Gamma = 1$. This will partially fill the channel form, decreasing levee height to re-equilibrate channel dimensions with smaller characteristic turbidity currents. If the concentration falls below the saturation concentration, there is excess suspension capacity that will lead to entrainment of sediment from the channel floor. This will increase the depth and cross-sectional area of the channel to re-equilibrate with the size of larger characteristic turbidity currents.

In conclusion, a diverse suite of concepts suggests that channel size and thickness of characteristic turbidity currents are related to each other, and this justifies the equation of channel depth and flow thickness ($H=D$) in the first order prediction of flow structures from channel dimensions.

Concentration: the Density of the Turbidity Current --- Robust first order predictability of concentration magnitude through wholly process-based equations in this simplified model framework is not yet feasible. The choice is therefore made here to make the average concentration a user-defined boundary condition, rather than set it through some empiric parameters behind the scenes of the SBE. This approach at least makes the concentration uncertainty clearly defined by the user at the front end of the model. The question now arises what typical concentrations are of turbidity currents.

The only reliable measurements of depth-averaged concentrations of real-world turbidity currents were published by Azpiroz-Zabala et al. (2017) and Simmons et al. (2020). They recorded very low concentrations of 0.017-0.023 % in 48-77m thick turbidity currents travelling down the Congo Canyon with a velocity of under 1 m/s. These conditions are likely to represent the slower end of the spectrum of turbidity currents in the Congo Canyon, though other measurement attempts of faster events have so far resulted in equipment failures (Khripounoff et al., 2003). Reliable average concentration measurements are not available for such faster natural turbidity currents in other systems either. Due to the near-complete lack of accurate concentration measurements in natural flows (Wang et al., 2020), various authors have tried to estimate average concentrations by combining other variables with equations. Konsoer et al. (2013) combine friction factor estimates with estimations of bank full conditions that are much like the perspective set out in the previous section. This leads them to estimate a sediment concentration range of 0.2-0.6% for a selection of channels exposed on the modern sea floor. Zeng et al. (1991) also applied friction factors to estimate sediment concentration during a turbidity current that occurred in May 1986 in the submarine channel in Bute Inlet (Canada). This turbidity current travelled at 3.6 m/s, resulting in a sediment concentration estimate of 0.5-0.7% (Zeng et al., 1991). These depth-averaged concentration values seem to be more representative for a broader range of active and ancient turbidity current systems than the very dilute concentrations reported by Azpiroz-Zabala et al. (2017) for the Congo Canyon. Indeed, a compilation by Sequeiros (2012) of concentration estimations from literature leads the author to suggest that 0.45% is a typical average concentration at field scale, consistent with both the range suggested by Konsoer et al. (2013), and the estimate of Zeng et al. (1991). Finally, the Grand Banks 1929 turbidity current was the single largest turbidity current event known to have occurred in modern times, and its size, velocity, and sediment concentration have historically been thought of as the upper limits of what is possible in oceans on Earth (Kuenen, 1952). The sediment concentration was estimated to be 1.1-2.9% (Plapp and Mitchell, 1966), an estimate that has recently been adjusted to 2.7-5.4% (Stevenson et al., 2018; see below). This upper concentration limit is consistent with the review by Sequeiros (2012), who suggests that the average sediment concentration of a turbidity current rarely exceeds 5%.

Based on these sources, we suggest the following broad subdivisions for the average input concentration in SBE simulations: very dilute [0.05-0.2%]; dilute [0.2-0.6%]; intermediate [0.6-2%]; high [2-5%], with the dilute range advisable as a default. Interestingly, Reginald Daly arrived at likely sediment concentrations of 0.3-0.6% in his rather brilliant 1936 paper, solely by applying deductive and partially intuitive reasoning (Daly, 1936).

The user defined depth-averaged concentration allows evaluation of the following integral in the model workflow:

$$\overline{C}H = \int_0^\infty C_b e^{-kz} dz \qquad (11)$$

Evaluation of the integral results in an expression of the decay constant *k*:

$$k = \frac{C_b}{\overline{C}} \frac{1}{H} \qquad (12)$$

The decay constant thus depends on flow thickness, and the ratio of near-bed concentration to average concentration. This ratio often appears in modelling studies of turbidity currents (Parker *et al.*, 1986; Halsey *et al.*, 2017). It is the simplest measure for the degree of density stratification in the turbidity current. It approaches 2 in many experiments (Parker *et al.*, 1987), while higher numbers have been proposed, and recently confirmed, for natural scale flows (Azprioz-Zabala et al., 2017 & Simmons et al., 2020). Note that the concentration profile as described by Eq. 6 asymptotically approaches 0 at an indefinite elevation above the channel floor; some of the sediment declared in the two boundary conditions $\overline{C}H$ is thus actually suspended above the bank-full elevation in the exponential concentration profile. The chosen structure of Eq. 11 therefore creates a small discrepancy between the average concentration between the channel floor and the bank full depth, and the average of Eq. 6 between these two levels. A similar effect occurs in the more common integral approach of Ellison and Turner (1959). We accept this minor discrepancy and claim that its effects will be negligible in highly stratified natural currents (see for example Fig. 3b).

Slope of the System --- The slope of a channel is well defined in medium-low resolution oceanographic datasets. In subsurface systems, the slope can be estimated from seismic datasets (Shumaker *et al.*, 2017; Beelen et al., 2019). If data does not allow the slope to be measured directly for a system, slope estimates can also be based on analogues from modern oceanography (Covault *et al.*, 2011; Prather *et al.*, 2016) or stratigraphic panels of outcrop systems (Johannessen & Steel, 2005;

Hubbard *et al.*, 2010; Daniels *et al.*, 2018). Compaction of clinoforms adds an extra source of uncertainty (Beelen *et al.*, 2019) that can be taken into account when setting the confidence bounds of the slope values. Helland-Hansen et al. (2016) qualitatively grouped system styles with different steepness (Helland-Hansen *et al.*, 2016), and quantifications of the slope steepness have also recently been reviewed (Patruno *et al.*, 2015; Patruno & Helland-Hansen, 2018). Based on these sources, users of the SBE could use the following classes if no slope data is available for their system of interest: Gentle: 0.5-1°; Intermediate: 1-2.5°; Steep: 2.5-6°; Very Steep 6-12°. The very-steep class appears to be relevant only for steep submarine canyon systems, such as the Var Canyon (Mulder *et al.*, 1998), the canyons in the Ebro and North Catalan margins (Amblas *et al.*, 2006; Lastras *et al.*, 2011), or some canyons on the North American Pacific Margin (Lee et al., 2002).

Bed Roughness --- The size of the coarsest sediment particles making up the bed determines the bed roughness, which provides a boundary condition needed to solve Eqs. 10, 9, and 2. The user is therefore required to supply an estimation of the coarse fraction of the sediment particles present on the channel thalweg. This data can be obtained from grain-size analysis of core-samples obtained from the channel under investigation. It can also be taken from samples within other parts of the system when the channel body itself has not been cored, though this approach could lead to under-estimation of the grain size in the channel thalweg. No grain-size samples may be available in exploration settings. Geologists will then generally be able to set likely values (250 µm; coarse sand; small pebbles; etc.) based on their understanding of the basin setting and the source area of the sediment (Reading & Richards, 1994; Richards *et al.*, 1998).

THE SEDIMENT FLUX [M³/S] AND BUDGET [KM³] MODULES

The equations, closures, and boundary conditions discussed above suffice to solve the first order velocity and concentration structure of the multitude of characteristic turbidity currents in channels. The aim of this work, however, is to use the model for calculations of sediment flux and sediment budget. The SBE executes each of these calculations for all of the turbidity currents resulting from the probabilistic sampling of the flow boundary conditions. In turn, the boundary conditions needed to complete these modelling steps are also supplied as ranges between likely minimum and maximum values by the user. These ranges are uniformly sampled in a user-defined number of steps during the execution of an SBE simulation.

From Flow Structure to Sediment Flux

The sediment flux per unit width by the characteristic turbidity current can be determined by multiplying the concentration at each elevation with the corresponding velocity and integrating from the bed to an elevation some distance above the channel (Plapp & Mitchell, 1960):

$$Flux_{1D} = \int_0^{\infty} c(z)u(z)dz \qquad (12)$$

The vertical coordinate is discretized in the SBE with steps of size Δz, such that this expression can be evaluated as the dot product of the concentration and velocity profiles multiplied by the vertical step size:

$$Flux_{1D} = c(z) \bullet u(z)\Delta z \qquad (13)$$

The units of this sediment flux per unit width are m^2/s. The channel cross-section is here simplified to a trapezoidal shape, consisting of a flat channel-thalweg section in the middle, and two channel margins on either side (Fig. 1c). The lateral channel-bank angle is user defined, but will be set to 10 degrees throughout this paper for simplicity. The estimation of the total sediment flux through the channel cross section follows an established procedure in fluvial processes and engineering (Chang, 1988): For each section in the trapezoidal cross section, we calculate a hydraulic radius, shear velocity, and velocity and concentration profiles. The resulting flux of Eq. 13 is multiplied by the section-width, and the section-fluxes are added to obtain the total sediment flux through the channel cross-section [m^3/s]. The section-method can be used to calculate fluxes through more sophisticated cross-sectional channel shapes, for instance by calculating turbidity current structures that represent more (e.g. 10) lateral channel sections within a single channel cross section. This is not pursued here, because this is deemed to only give second order improvements in predicting the sediment flux at the cost of an order of magnitude increase in amount of turbidity current structures that need to be calculated. The added demand on the specificity of boundary condition constraints, in this case the channel cross-sectional shape, is also contrary to the philosophy of the SBE.

From Sediment Flux to Sediment Budget

The sediment supply to deep-water sedimentary systems is punctuated on the time scales of events and geological cycles (Romans *et al.*, 2016). The geological sediment budget need to be calculated by multiplying sediment flux of the characteristic turbidity currents with the typical duration of a typical flow event, its frequency, and the (geologic) time-scale of the system's activity.

Turbidity Current Duration --- Turbidity currents have commonly been estimated to last minutes to hours (Piper et al., 1988, [minimum 2 hours]; Allen, 1991, [20-52 minutes]; Baas et al., 2000, [16-19 minutes]; Jobe et al., 2012, [3-176 minutes]; Jobe et al., 2017, [minimum 6-12 minutes]; Stevenson et al., 2018, [4-8 hours]). Measurements of turbidity currents indicate that flows last minutes on proximal delta slopes (Hughes Clark, 2016). The majority of monitored flows in upper canyons, however, last between 1-10 hours (see Talling et al., 2013 for a review). Measurements in the Congo Canyon, which is the only of the major passive-margin deep water systems that is presently active, show that flows last up to 10 days 170 km away from the canyon head at water depths of 2000 m (Cooper, 2013; Azpiroz-zabala *et al.*, 2017). This longer flow duration in a major canyon system is consistent with the estimation for the Pleistocene Amazon flows by Pirmez and Imran (2003). They estimated that flows lasted several days in the Pleistocene phase of activity of the Amazon fan. These measurements and estimations are in line with the suggestion by Azpiroz-Zabala et al. (2017) that turbidity current duration is a function of distance from the source area of the flows and the stretching of flows as they transit down the system. The transit time of a flow towards a location in the basin allows the flow to stretch due to different velocities in different parts of the flow. Flows therefore last longer further away from the source, and similarly they last longer in the distal sections of larger systems. Even the very long turbidity currents measured in the Congo Canyon can be explained in this way without invoking a sustained source mechanism (Azpiroz-Zabala et al., 2017). The timescale of duration of turbidity currents at a location can thus be estimated by dividing the distance to the source area by a characteristic stretching-velocity scale of the currents. The estimation of the stretching velocity scale might require an iterative procedure where the SBE is initially used to reconstruct velocity profiles, which are subsequently used to evaluate the turbidity current duration boundary condition for sediment budget estimations. An alternative workflow in ancient and subsurface cases, where uncertainties are inherently large, might be to set broad ranges of turbidity current durations based on the geological setting: minutes to 1 hour for delta slopes; hours to 10 hours for canyons in the upper continental slope and slope channels in smaller basins with steep slopes; 10 hours to a few days for larger canyons in the lower continental slope; and a few days to a week for distal parts of large (~1000 km long) submarine fans.

Recurrence Time --- Recurrence times of turbidity currents are increasingly well constrained in literature (Piper & Deptuck, 1997; Pirmez & Imran, 2003; Xu, 2011; Talling *et al.*, 2013; Clare *et al.*, 2014, 2016; Stevens *et al.*, 2014; Azpiroz-Zabala *et al.*, 2017; Allin *et al.*, 2018; Jobe *et al.*, 2018; Stacey *et al.*, 2019). Much direct monitoring evidence points to a few to many tens of turbidity currents being generated each year at the top of the slope in active systems. This activity can be bundled seasonally in summer in response to meltwater hydrographs (Clare *et al.*, 2016; Hizzett *et al.*, 2018), or winter in response to storm activity (Xu *et al.*, 2004; Pope *et al.*, 2017). These very short recurrence times rapidly increase down-slope (Stevens *et al.*, 2014; Stacey *et al.*, 2019), because many turbidity currents dissipate within the slope system (Heerema *et al.*, 2020), which is thus a staging area for sediment that is only occasionally exported all the way to the basin floor by large, fan-building turbidity currents (Jobe *et al.*, 2018). Recurrence time of turbidity currents thus depends highly on the position in the system of interest, the mechanism that ignites these flows, and the size of the shelf itself. Consequently, flow frequency can vary from weekly to monthly or seasonal event in low storage capacity (short) shelves, to decadal, centennial, or even millennial -scale recurrence intervals in high storage capacity (broad) shelves, especially if these flows are triggered through geologic factors like the Grand Banks earthquake rather than fluvial flooding as per the Congo system. In summary, if upper slope sedimentation is of most interest, the shorter recurrence times are advised as input. If sediment export to submarine fans at the base of slope is of interest, recurrence times of decades to centuries can be appropriate (see Jobe et al., 2018, for compilations of recurrence times in dated Quaternary fan systems), though evidence suggests that turbidity currents travel down major channel-levee systems, such as the Amazon, annually during periods of glacioeustatic lowstands of sea level (Piper & Deptuck, 1997; Pirmez & Imran, 2003). The largest millennial recurrence times seem to be restricted to systems where turbidity currents are triggered by rare seismic events (Clare *et al.*, 2014).

If recurrence times for ancient examples are considered too uncertain to set as an input condition, an alternative strategy is to enforce an event count, based on stratigraphic evidence, by the combination of recurrence time and duration of system activity.

Allocyclic System Activity --- The duration and recurrence time of turbidity currents are both aspects of the short timescale punctuation of submarine channel activity. Punctuation of activity also exists on longer timescales. This long timescale punctuation of activity generally relates to external, or allogenic, forcing that causes periodic attachment and detachment from the feeder systems of the submarine depositional system (e.g. shelf-edge deltas; litoral cells; or estuaries).

Classic sequence stratigraphy incorporates the best-known concept for external forcing of punctuated deep water activity (e.g. Posamentier and Vail, 1988). It describes how deep-water systems are mostly sediment-starved during periods of relative sea-level highstand, when basin margins are generally flooded and the sediment budget that is brought to the basin margin by rivers is mostly deposited in coastal plain and deltaic environments on the shelf. Deltas prograde to the shelf edge during subsequent periods of relative seal-level lowstand. The shelf-edge deltas are positioned at the top of the slope leading into the deep basin, such that sediment accumulated in these deltas can easily be mobilized to trigger turbidity currents (Daly, 1936). This concept has been validated on various deep-water systems around the world, especially for the Pleistocene era (Anderson, 2000; Sylvester, 2012). In lowstand-dominated systems, the deep-water system activity duration should therefore be set by the user to the phase within the dominant geological cycle during which shelf-edge deltas are present. The precise timing of this phase has been determined for the Eastern Gulf of Mexico (Pirmez et al., 2012) and the Niger Delta slope (Jobe et al., 2015). Pirmez et al. (2012) document that sedimentation in the Brazos-Trinity system in the Gulf of Mexico took place mostly in the 9 kyr period from 24-15 ka, around the maximum sea-level lowstand in the latest Late Glacial Maximum. In the case of the Niger Delta system, Jobe et al. (2015) documented how one of the prominent channel conduits was abandoned during the sea level rise at the end of the second-last glacial, at 130 ka. Sandy turbidity current activity resumed at 50 ka, concurrent with the sea level fall in Marine Isotope Stage 3. The activity lasted through the glacial sea level lowstand until the channel system was abandoned again in two steps from 19-15 ka. The system activity thus lasted ~30-35 kyr within a ~100 kyr glacioeustatic cycle. The SBE should primarily be used to determine the sediment budget for these active phases of sediment delivery in deep marine systems.

The human mind is naturally prone to project situations that it knows best as the norm onto the unknown. For geologists this leads to a Pleistocene-projection bias, a pitfall that entails regarding the present-day ice-house setting as the norm for the geological past. Many deep-water depositional systems of interest were active in Jurassic, Cretaceous, or Paleogene times, when fluctuations of relative sea-level are generally believed to have been less prominent as a forcing of sediment supply to deep-water depositional systems (Blum and Hattier-Womack, 2009). In such systems climate is operating through mechanisms other than glacio-eustacy, for instance by forcing sediment production and transport cycles on the continents (Carvajal and Steel, 2006; Zhang et al., 2019). Interestingly, the time scale of climatic forcing of sediment supply to deep marine basins appears to be of order 10-100 kyr, which is similar to glacio-eustatic lowstand re-occurrence times (Carvajal and Steel, 2006; Crabaugh and Steel, 2004; Grundvåg et al., 2014; Burgess and Hovius, 1998; Blum & Hattier-Womack, 2009). In such cases the system activity parameter of the SBE should be set to the length of time within the climatic cycle that characterizes the phase of maximum regression of deltas to the basin margin.

The considerations above are tailored to low-gradient systems on non-glaciated, tectonically passive margins. Geologists must be willing to depart from this established standard model that has been tailored to such a specific basin-setting when the context suggests to do so. For instance, it has been shown that the effect of sea-level fluctuations on deep water sediment delivery can be fundamentally different in steep, tectonically active systems characterized by a narrow shelf (Covault *et al.*, 2007). Covault et al. (2007) documented how sediment derived from part of Southern California is predominantly delivered to submarine fans during sea level highstand, when the Oceanside littoral cell is at its peak activity and generates a high supply of sediment to the la Jolla Canyon head. The Congo Canyon system is another example that does not follow the sea-level lowstand paradigm (Khripounoff *et al.*, 2003; Azpiroz-Zabala *et al.*, 2017) due to the direct connection that exists between the Congo Canyon head and the Congo Estuary. These examples illustrate that general rules of allocyclic activity must be released if particular aspects of the basin configuration invalidate them.

SBE-RESULT STRUCTURE AND SENSITIVITY ANALYSIS

The structure of the default SBE results is illustrated with a simulation of a hypothetical system characterized by dilute turbidity currents (C=0.2-0.6%), down intermediate slopes of 1-2.5°, through channels with dimensions of width and depth spanning 200-400 m and 10-20 m respectively. The median grainsize of the channel bed is 150 μm, and the coarse sediment (d_{90}) is 350 μm. Currents last a few hours (2-4), and deliver sediment to the base of slope once every 10-20 years during a maximum regression that lasts 5-10 kyr (see Table 1 for an overview of conditions). Figure 3 displays the default results of the SBE run with these input conditions. The velocity and concentration profiles of all simulated turbidity currents are stored by the SBE, but for simplicity only the profiles of a single simulated turbidity current are displayed as an example (Fig. 3a&b). This example simulation is picked from the characteristic turbidity currents whose maximum velocity is closest to the mean of all simulated maximum velocities. This procedure means that the displayed example profiles do not necessarily result from the mean boundary conditions. They may reflect, for instance, thicker or thinner flows that combined with changes in the other boundary conditions result in a maximum velocity that lies close to the mean of maximum velocities in all simulations.

The turbidity currents in this hypothetical system have a maximum velocity of ~3 m/s, are highly stratified with a maximum concentration near the bed of ~6%, transport ~15 m^3 of sediment every second, which amounts to ~0.1 km^3 of sediment per cycle (Fig. RefCase). These results will not be analyzed in detail, but serve as the reference to a) explore the sensitivity of the simulation results to uncertainty of the input conditions, and b) the response of the results to changing input conditions.

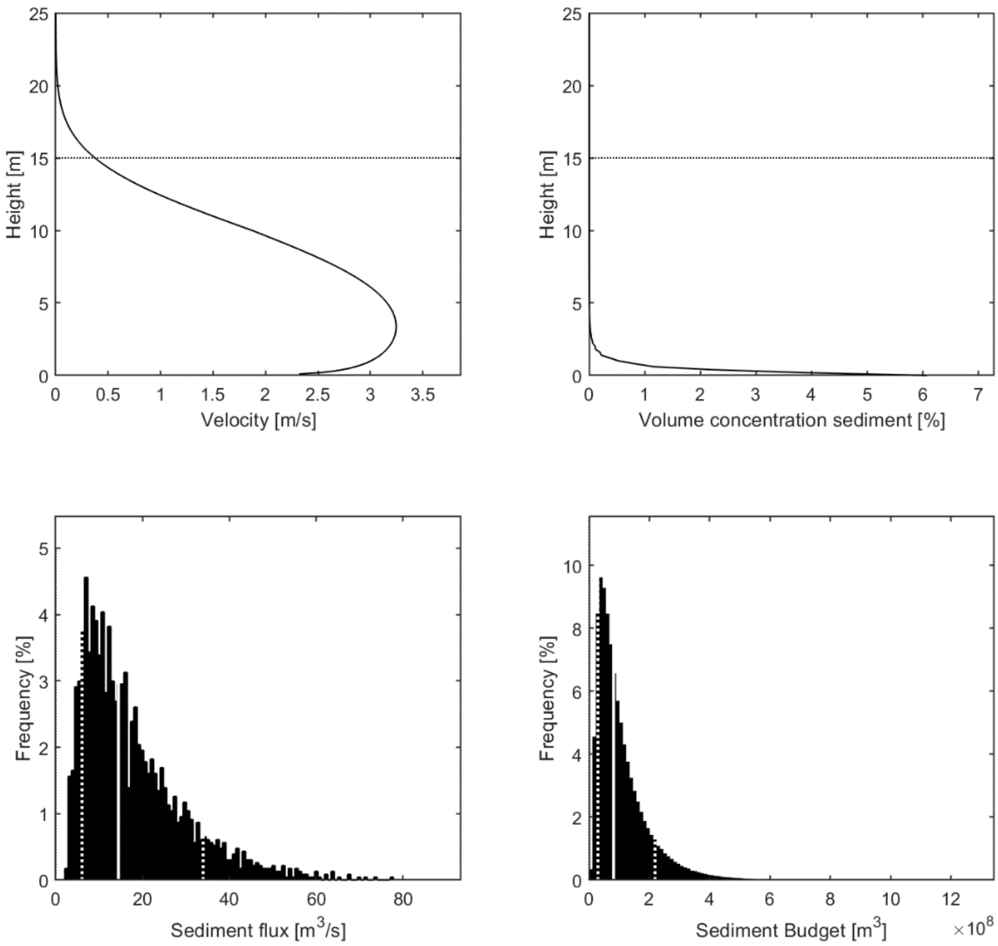

Fig. 3: *SBE default results for the base case simulation [Table 1]. A&B) Velocity and concentration profiles of a characteristic turbidity current in the base case system. Horizontal dotted line indicates the mean input channel depth for reference. Note that the displayed example was thinner than the mean thickness. C) Histogram of sediment flux (m^3/s) through a characteristic channel cross section. D) Histogram of sediment budget of the system over a full cycle of activity. Vertical white line indicates the p_{50} of predicted sediment budgets, white dotted lines indicate p_{10} and p_{90}.*

The sensitivity of the SBE to changes in input conditions is tested by reducing the uncertainty of all input variables, apart from one, to +/-1% of the mean of the base case input range. The simulation is repeated with the uncertainty of a single different variable reinstated each time. The sediment budgets of all the simulations are displayed in order of descending spread of the predicted sediment budgets (Fig. 4), in a so-called tornado diagram (Holbrook & Wanas 2014; Lin & Battacharya 2017). These diagrams reflect the sensitivity of the model output to the uncertainty of the variables used as input conditions. The average input sediment concentration comes out as the variable with most impact on the simulation results (Fig. 4a); most of the spread of the base case is maintained when all variables apart from the sediment concentration are set to range +/-1% around the mean of the base case input. Channel width also has a relatively large impact on the spread of the sediment budget results, but is a distant second to the sediment concentration parameter. The three temporal parameters in the SBE (flow duration, frequency and system activity) show an identical and moderate influence on the spread of the sediment budget. Channel depth, interestingly has a smaller impact on the total uncertainty. The insensitivity to uncertainty in slope of the system is striking: the spread of predicted sediment budgets is reduced to a narrow range while the slope is still varied from 1° to 2.5° (Fig. 4a). There is thus very little benefit to be gained from increasing the confidence levels of slope estimates. This is a somewhat unexpected result due to the importance generally attributed to slope in the literature (Kneller, 2003; Stevenson *et al.*, 2015; Pohl *et al.*, 2020).

Achieving uncertainty levels of +/-1% is unrealistic in natural turbidity current systems. Another tornado diagram is therefore produced for which uncertainties in all variables apart from one have been reduced by 50% (Fig. 4b). This diagram confirms the sensitivity ranking of variables that was found in Fig. 4a. It also shows that the spread in sediment budgets in most simulations is rather equal to that of the simulation where uncertainty in all variables has been reduced by 50% (Fig. 4b). This result indicates that it is acceptable for relatively high uncertainty to remain in one or two of the intermediate-sensitivity input parameters. There is little benefit in spending much effort on reducing that uncertainty of a single variable, because the spread in sediment budgets will remain similar even if it’s uncertainty is reduced by 50%. The exception to this is the input sediment concentration: even if all other variables are set to a 50% reduction of uncertainty, the spread of results does not decrease much (Fig. 4b), which again points to the importance of uncertainty about sediment concentration in turbidity currents.

As a final exercise in this section, the base case is repeated with the input range doubled for one variable at a time. The duration, frequency, and system activity all have a linear relation with the sediment budget, and doubling these variables results in doubling of the simulated sediment budgets (Fig. 4c). Channel width and sediment concentration both have a nonlinear effect. The concentration again has the largest impact with the predicted sediment budgets quadrupling as a result of the doubled input range. Channel depth has a subdued effect, and doubling of the slope range from 1-2.5° to 2-5°, a dramatic increase in slope within the band-width of natural slope angles, merely has the effect of increasing the spread of predicted sediment budgets somewhat.

621

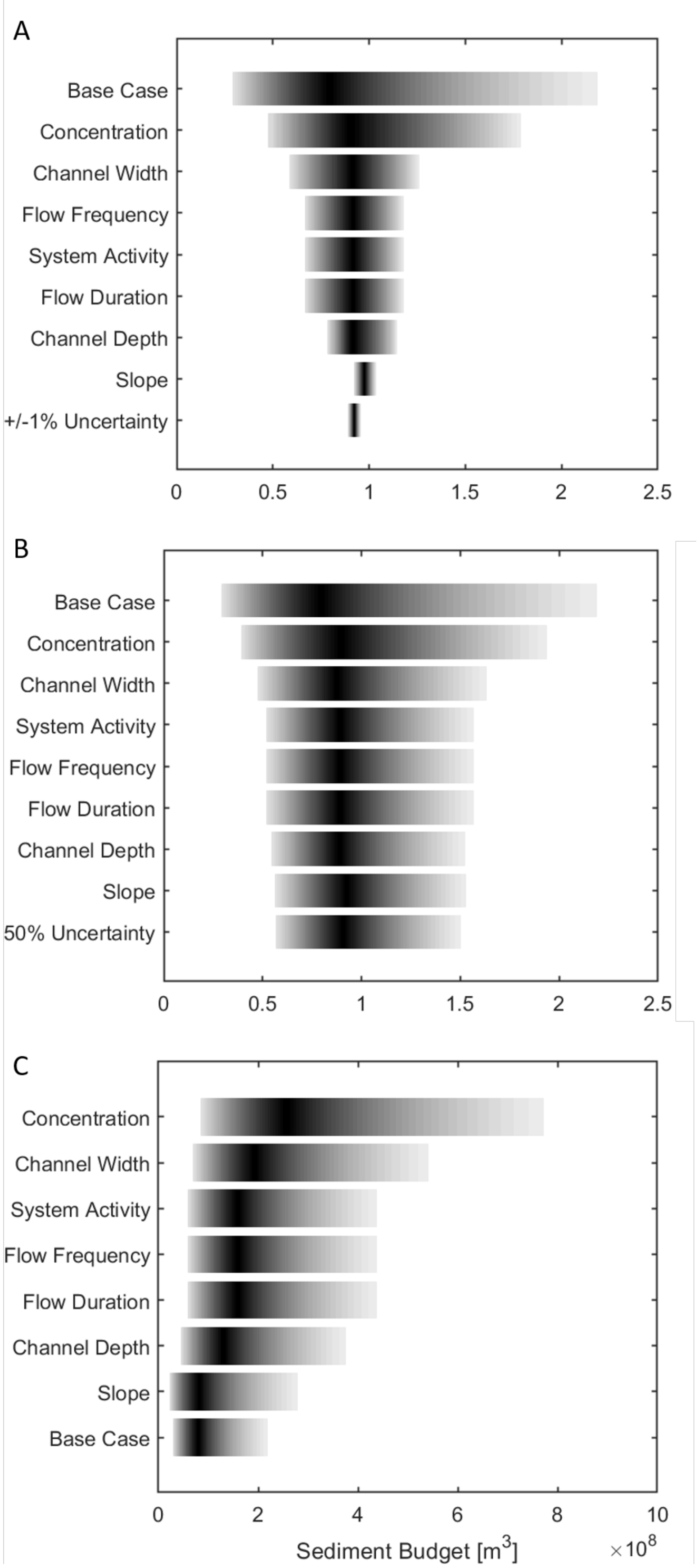
A
Base Case
Concentration
Channel Width
Flow Frequency
System Activity
Flow Duration
Channel Depth
Slope
+/-1% Uncertainty
0
0.5
1
1.5
2
2.5
B
Base Case
Concentration
Channel Width
System Activity
Flow Frequency
Flow Duration
Channel Depth
Slope
50% Uncertainty
0
0.5
1
1.5
2
2.5
C
Concentration
Channel Width
System Activity
Flow Frequency
Flow Duration
Channel Depth
Slope
Base Case
0
2
4
6
8
10
Sediment Budget [m3]
×10^8

Fig. 4: *Tornado diagrams of sensitivity analyses of the SBE results. Base case conditions are given in Table 1. A) Uncertainty in all variables apart from 1 is reduced to +/-1% of the mean input of the base case. Uncertainty of all variables was reduced in the "+/-1% Uncertainty" scenario. B) Uncertainty of all variables apart from one was reduced to 50% of the uncertainty in the base case. Uncertainty of all variables was reduced in the "50% Uncertainty" scenario. C) Input range of a single variable was doubled compared to the base case. The gray scales changes from black for p_{50} to light gray for p_{10} and p_{90}.*

VALIDATION OF THE MODEL

We validate the SBE app here with examples of the smallest and largest scale turbidity currents on earth for which detailed data is available: laboratory turbidity currents and the 1929 Grand Banks turbidity current.

Laboratory Turbidity Currents

Boundary Conditions --- The model is tested on Run 3 of de Leeuw et al. (2018b). This experiment was selected because it displayed the least amount of in-channel and levee deposition of all the experiments reported in that paper. It was therefore most representative of a bypassing channel, indicative of the flow-channel size equilibrium discussed in section 2.3, above. In fact, the size of the pre-formed channel resulted in a phase of initial channel deepening and widening (Fig. 5a), which indicates that the channel dimensions were smaller than the dimensions in equilibrium with the characteristic turbidity current initiated by de Leeuw et al. (2018b). The velocimetry data shows that channel deepening took place in the initial 40 seconds of the experiment, after which the channel thalweg stays at a constant elevation throughout the final 40 seconds of the experiment (Fig. 5b). This is interpreted here to indicate that the initial erosive channel enlargement led to an equilibrium between the turbidity current and the channel dimensions. The channel dimensions used as input for the SBE are there for obtained from the digital elevation model of the topography measured after the experiment. The full list of input conditions for the SBE are displayed in Table 1. The uncertainty ranges for the input conditions have been determined by applying an error margin of +/-10% to the best guess values, which is appropriate for controlled sedimentology experiments.

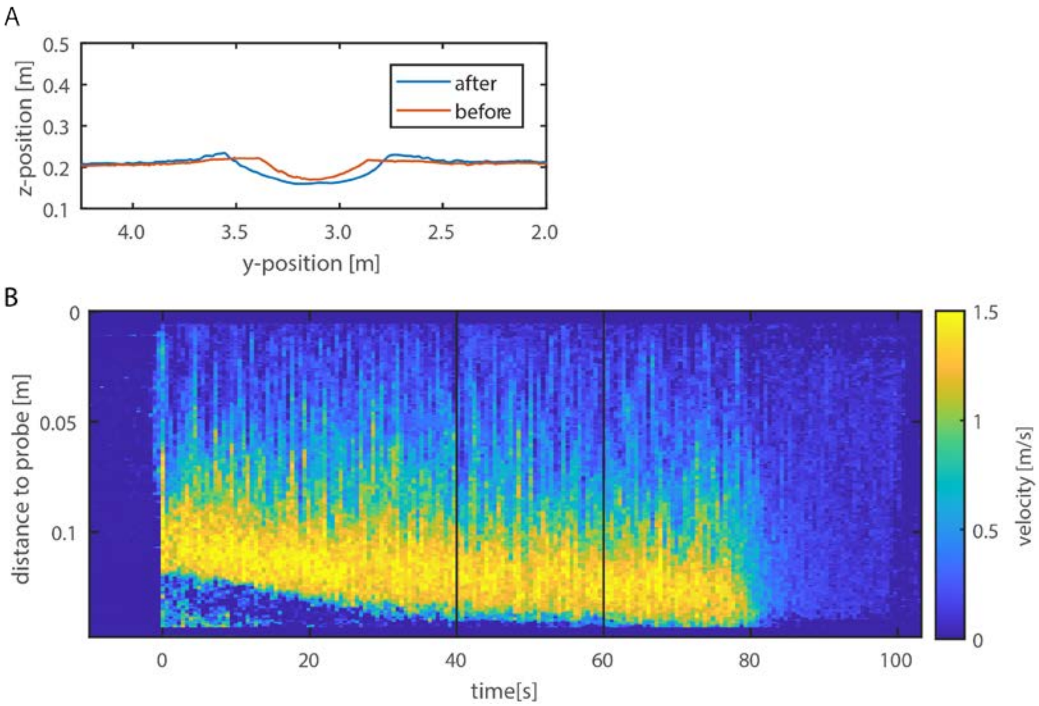

Fig. 5: *A) Channel cross-sections measured before and after Run 3 of de Leeuw et al. (2018b). B) Velocity of the experimental turbidity current measured at the channel thalweg measured with an Ultrasonic Velocimetry Profiler (UVP). The distance from the high-velocity core of the turbidity current to the UVP probe increases during the first 40 seconds of the experiment, which indicates erosion of the channel thalweg. Vertical black lines indicate the 20 s averaging window used for validation of the SBE velocity profile.*

Results --- The predicted velocity profiles match the UVP measurements quite closely (Fig. 6a). The velocity maximum is predicted precisely (1.36 m/s). The elevation of the velocity maximum is predicted at a higher position in the SBE compared to the experimental measurements (3.2 cm vs. 2.4 cm). Also, the velocity in the mixing layer was more asymmetrical in the experiment compared to the SBE velocity profile. The predicted concentration profile has elevated concentrations near the base and decreased concentrations towards the top compared to the average input concentration (Fig. 6b). The predicted basal sediment concentration reaches the maximum granular concentration due to the high bed shear stress. The actual experimental sediment budget does fall within the range of predicted values (Fig. 6c&d), albeit at the very low end of the distribution, around the first percentile value (p_{01}). The p_{50} values of predicted flux and budget are 80% overestimated by the SBE compared to the actual experiment.

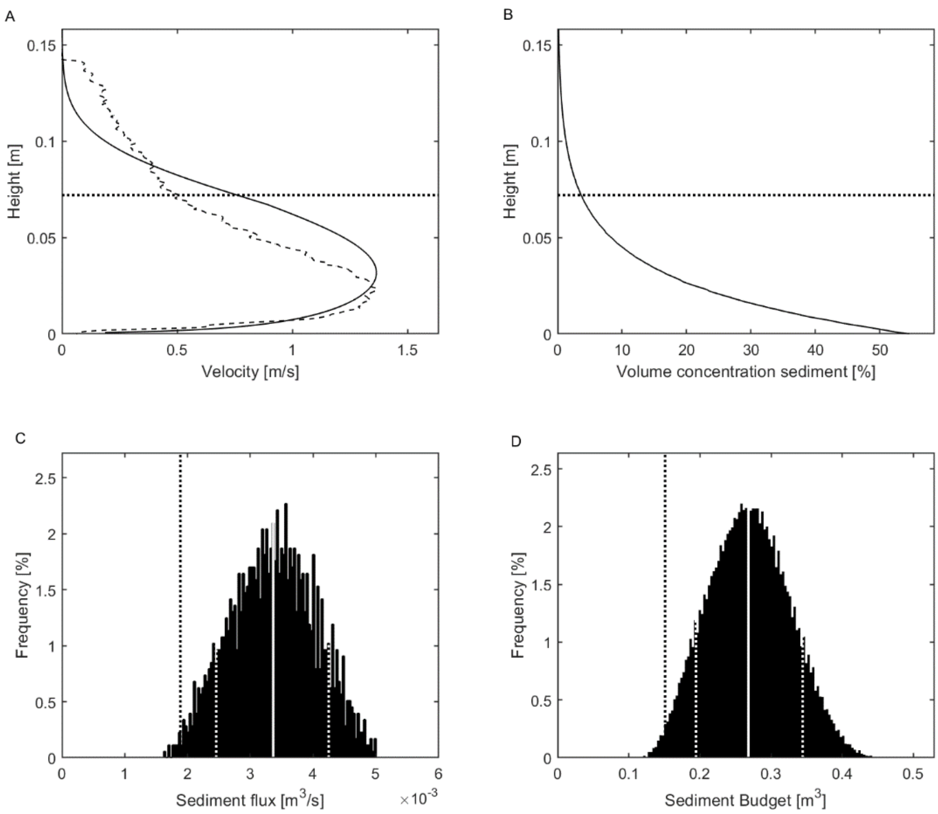

Fig. 6: *Results for the SBE simulation of Run 3 of de Leeuw et al. (2018). A) Velocity profile resulting from the SBE (solid line); measured velocity profile (dashed line). Horizontal dotted line indicates channel confinement depth. B) Concentration profile resulting from the SBE. C) Simulated range of sediment flux. Black dotted line indicates sediment flux of the experiment (1.9*10*$^{-3}$ *m*^{3}*/s). White vertical line indicates the median of the reconstructed sediment fluxes (3.4*10*$^{-3}$ *m*^{3}*/s); dotted lines indicate 10*th *and 90*th *percentiles of reconstructions. D) Reconstructed sediment budget. Black dotted line indicates the amount of sediment supplied to the mixing tank in preparation of Run 3 of de Leeuw et al. (2018b; 0.15 m*^{3}*). White vertical line indicates the median of the reconstructed sediment budgets (0.27 m*^{3}*); white dotted lines indicate 10*th *and 90*th *percentiles of simulated budgets.*

Evaluation --- Estimations of the error margins of UVP measurements do not exist, but the prediction of the maximum velocity can clearly be qualified to be within the margin of this error. The elevation of the velocity maximum and the inability to capture the asymmetry of the mixing layer are here classed as mismatches of secondary importance. These discrepancies could point to the 2nd order importance of the density profile, which is assumed to be negligible in both the law of the wall (Eq. 2) and the plane mixing layer structure (Eq. 3) applied in the SBE. Improvements of the velocity profile function is not pursued here because even though this output is informative and interesting, it is merely a necessary step to obtain the key sediment flux output of the SBE.

The actual experimental sediment budget equals the 1st percentile value of the distribution of predictions, and the p_{50} of the predictions overestimates the sediment budget by 80%, which is within the factor of 2, the expected level of accuracy of any sediment transport flux estimations obtained from comparatively simple and tightly controlled open-channel flows (Chang, 1988). The very high predicted basal sediment concentrations are likely a major contribution to the overestimation of the sediment budget. The concentration profile was not measured by de Leeuw et al. (2018b), but concentrations obtained by siphoning similar turbidity currents in another set-up suggest that basal sediment concentrations reach ~30% (e.g. Pohl et al., 2020), not the 50+%

predicted by the SBE. Another major contributor could be the eroded sediment added to the turbidity current in excess of the budget supplied from the mixing tank, which is estimated to have supplied ~60 liters of sediment (an average of 3 cm erosion over a 0.8 m wide 4 m long channel section). Aditon of this eroded sediment to the experimental sediment budget would raise it to ~0.21 m^3, just above the p_{10} value of the simulated population. Furthermore, scrutiny of the logbook of the experimental procedure of the experiment that was simulated here also revealed that the volume of water supplied to the mixing tank could have been as much as 0.928 m^3, and that 28 kg of sediment has been recorded to remain in the pump & pipe system that supplies the mixture to the Eurotank. While the sediment in the pipes lowers the eperimental sediment budget slightly, in combination with the elevated water volume it implies that the actual experimental sediment concentration could have been as low as 15% instead of the intended 17%. The sensitivity analysis (Fig. 4c) suggests that this lower actual concentration would have a marked effect to decrease the SBE-predicted sediment budgets.

A number of improvements to the prediction could be pursued by tailoring the SBE more closely to the laboratory experiments. However, all such improvements would necessarily entail using more intricate boundary conditions, and go against the idea of the SBE as a robust tool to be used across a range of scales when information about the system is sparse. Furthermore, it is not very satisfying or useful to optimize a model for predictions at laboratory scale before investigating how it performs for real world cases. Fitting the SBE more closely to laboratory experiments will therefore not be pursued here. Instead we will investigate the validity of the SBE across scales by turning our attention to the largest turbidity current for which measurements are available: the 1929 Grand Banks turbidity current.

	Base Case	Eurotank Experiment	1929 Grand Banks Event
Channel Width [m]	200-400	0.82 +/-10%	23000 +/-10%
Channel Depth [m]	10-20	0.072 +/-10%	201 +/-10%
System Slope [°]	1-2.5	11 +/-10%	0.45 +/-10%
Thalweg grainsize (d_{50}; d_{90}) [$*10^{-6}$ m]	150; 350	131,223	1250; 5000
Sediment Concentration [%]	0.2-0.6	17 +/-10%	Ref. 2.7-5.4 High 5.4 +/-10% Low 2.7 +/-10%
Current Duration [h]	2-4	80/3600 +/-10%	4-8
Current Frequency [-/yr]	0.05-0.1	1	1
System Activity [kyr]	5-10	0.001	0.001

Table 1 *Input parameters for the SBE simulations of a hypothetical base case, EuroSEDS experiments, and the 1929 Grand Banks turbidity current.*

Validation against the 1929 Grand Banks turbidity current

Boundary Conditions --- The 1929 Grand Banks turbidity current is the largest scale event, in terms of volume of sediment transported, for which data on bathymetry, flow velocity, flow thickness, and flow composition is available (Heezen & Ewing, 1952; Piper & Aksu, 1987; Piper *et al.*, 1988; Hughes Clark *et al.*, 1990; Krastel *et al.*, 2016; Stevenson *et al.*, 2018). It has long been used as a testing ground for models of turbidity current dynamics (Kuenen, 1952; Plapp & Mitchell, 1960; Stevenson *et al.*, 2018). Insights from the 2015 RV Maria S. Merian cruise (Cruise No. MSM47; Krastel *et al.*, 2016; Stevenson *et al.*, 2018) are used here to constrain the SBE. The aim of this exercise is to validate the velocity and concentration results of the SBE and establish how the range of sediment budget estimates from the SBE relates to the estimated volume of 175-185 km^3 of the deposit that was formed on the Atlantic abyssal plane during this event (Piper & Aksu, 1987; Piper *et al.*, 1988).

The boundary conditions for the simulation of the Grand Banks turbidity current are set using a combination of parameters measured in the field and reconstructed flow properties such as sediment concentration (from Stevenson et al., 2018). Channel bathymetry at Transect 2 across the Eastern Valley provides constraints on flow thickness (201 m), channel width (23,000 m) and slope (0.45°). Cable breaks across this part of the slope measured the flow speed to be 19.1 m/s (Heezen & Ewing, 1952). From these data the depth-averaged sediment concentration of the flow was reconstructed between 2.7-5.4 % by volume (Stevenson *et al.*, 2018). Given these input conditions (Table 1), the SBE model outputs include a prediction of the overall sediment budget of the flow. This parameter is constrained by deposits mapped out in the field, whereby approximately 70 km^3 of sediment passed through Transect 2 of the Eastern Valley (Stevenson *et al.*, 2018). The rest of the 175-185 km^3 deposit on the abyssal plane was transported along other flow-pathways on the Grand Banks continental slope.

Results --- First, we present model outputs using input conditions from Transect 2 (Table 1) with sediment concentrations of 2.7-5.4 % (reconstructed by Stevenson et al., 2018). The SBE model shows remarkable agreement with the observed and reconstructed properties of the 1929 Grand Banks deposit and flow (Fig. 7). The velocity profile of a representative simulated flow shows a velocity maximum being slightly higher than 20 m/s, which is consistent with the velocity of 19 m/s deduced from the timing of cable breaks (Fig. 7a). The concentration profile indicates a highly stratified dense basal flow with high concentrations (>10%) up to ~25m from the bed, overlain by a low-density cloud (Fig. 7b).

The predicted sediment flux through the channel at Transect 2 was ~$3*10^6$ m^3/s (p_{50}; Fig. 7c), an order of magnitude more than the water discharge of the Amazon, which is largest river on Earth by discharge. This flux is combined with an estimated 4-8 hour flow duration (Stevenson *et al.*, 2018). The model then predicts a p_{50} of deposit volume of 60 km^3 with a p_{10}-p_{90} range between ~30 and ~100 km^3 (Fig. 7d).

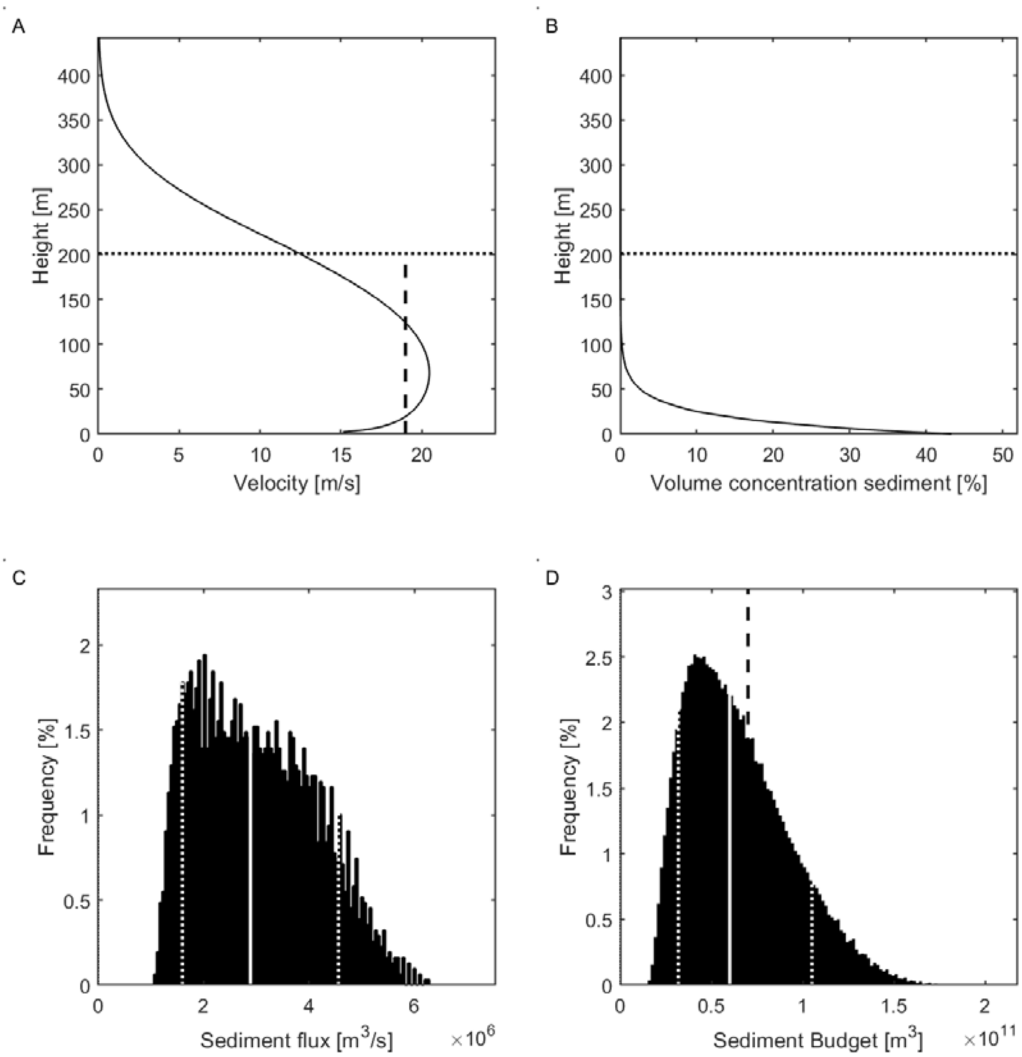

Fig. 7: *SBE results of the Grand Banks 1929 turbidity current reconstruction. A&B) Representative velocity and concentration profiles. Horizontal dotted line indicates flow thickness from Stevenson et al. (2018). Vertical dashed line indicates velocity based on the timing of cable breaks (Heezen & Ewing, 1952). C) Sediment flux. Vertical white line indicates the p_{50} of predicted sediment flux, white dotted lines indicate p_{10} and p_{90}. D) Simulated sediment budget of the flow through Transect 2. Vertical white line indicates the p_{50} of predicted sediment budgets, white dotted lines indicate p_{10} and p_{90}. Vertical black dashed line indicates estimated sediment budget of the Eastern Valley (70 km^3).*

Evaluation --- The input sediment concentration used had a broad range from 2.7-5.4%, and it was shown in the general sensitivity analysis that this can impact the SBE results to a great extent (Fig. 4). To explore the validity of these results we first present a sensitivity analysis on the sediment concentration parameter. Simulations were repeated with all parameters except the concentration kept the same; the concentration range was adjusted to the lower end and upper end of the estimates by Stevenson et al. (2018), each with a +/-10% uncertainty (Table 1). Low sediment concentrations of 2.7% result in flow velocities of ~15m/s (Fig. 8). In contrast, using a high sediment concentration condition of 4.9-5.9% results in flow velocities of ~23 m/s. The low and high end of Stevenson et al.’s (2018) concentration reconstructions thus result in under- and over-estimation of the Grand Banks velocity respectively. A concentration value midway between 2.7 and 5.4% (~4 %) produces flow velocities very similar to the values measured in the field (Fig. 7b). At the same time this result validates the velocity function of the SBE and the sediment concentration reconstruction by Stevenson et al. (2018). It is worthwhile emphasizing that the sediment concentration range was estimated by Stevenson et al. (2018) based on Chézy friction equations. This Chézy calculation output is used as an input constraint in the SBE simulation. The success of the present analysis should therefore not be seen as an independent validation against measurements only. Rather, the SBEis a corroboration of Chézy approaches (Middleton, 1966; Zeng *et al.*, 1991; Konsoer *et al.*, 2013; Stevenson *et al.*, 2018; Simmons *et al.*, 2020), while modelling the effects of the mixing layer through a technique rooted in fluid mechanics (Pope, 2000) rather than empirical coefficients. Stevenson et al. (2018) also estimated flow duration by dividing the sediment budget transported through the Eastern Valley by average velocity and concentration. This yields an estimated flow duration of 4-8 hours. This flow duration was used in the SBE Grand Banks simulation (Table 1). The range of calculated sediment budgets is centered around the 70 km^3 observed in the field. Though this result seems remarkable it adds little to the validation of the velocity and concentration scales because the SBE procedure is simply the inverse of the duration calculations performed by Stevenson et al. (2018). It does illustrate, however, how the SBE quantifies the effects of remaining geologic uncertainties explicitly by reconstructing a histogram of likely sediment budgets, with a p_{10}-p_{90} range of 30-100 km^3, centered on the remarkable volume of 70 km^3 sediment transported through Transect 2 of the Eastern Valley during the Grand Banks event (Piper et al., 1988; Stvenson et al., 2018).

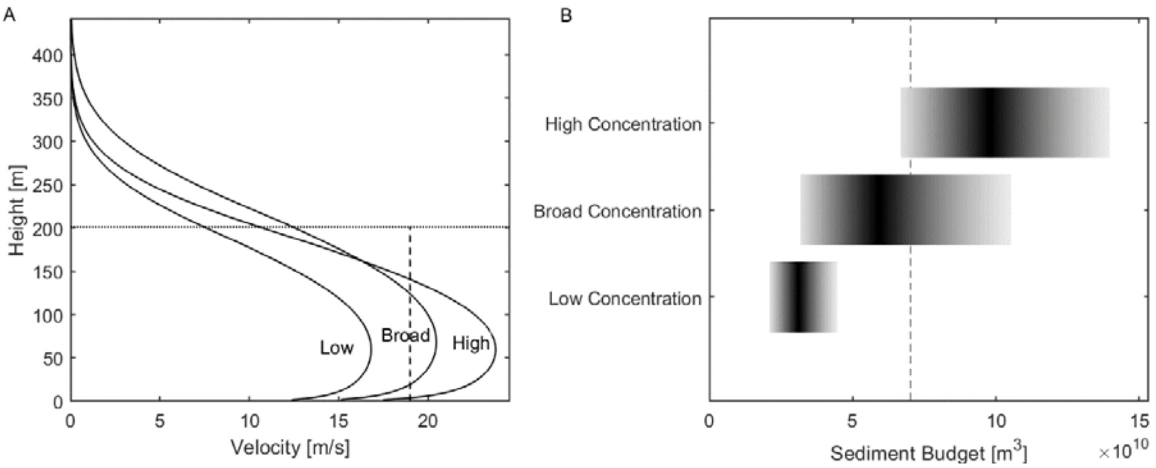

Fig. 8: *A) Examples of characteristic velocity profiles obtained for low concentration estimate (slow flow), broad concentration estimates (intermediate flow), and high concentration estimates (fast flow). Vertical dashed line indicates cable break velocity. B) Simulated sediment budget ranges for the three concentration ranges (see Table 1). Gray scale changes from black at p_{50} to light fray at p_{10} and p_{90}. Vertical dashed line indicates observed 70 km^3 sediment budget.*

Validation discussion: The smallest and the largest.

Heezen and Ewing (1952), and Kuenen (1952) perceived the recording of the 1929 Grand Banks event by cable breaks as a turbidity current experiment at the largest scale possible on Earth. The Eurotank experiments represent the smallest scale at which turbidity currents can be studied with natural sediments, a fluid with the viscosity of water at room temperature, and with a gravitational acceleration of 1**g*. The SBE performs within standard acceptable accuracy of sediment flux predictors in these validations in isolation. It is remarkable that the SBE achieves this level of success at the smallest and largest scales possible on planet Earth, which are separated by 12 orders of magnitude, without any changes in parameterizations or the equations themselves. There is apparently no application on Earth that is outside the range of scales for the SBE, and no need to apply it outside the range for which it is established. This robustness of the SBE encourages us to seek applications of the SBE in cases where it is predictive without the possibility of validation.

APPLICATION OF THE SBE TO AN ANCIENT CHANNEL DEPOSIT IN OUTCROP

The slope channels of the Cretaceous Tres Pasos Formation (Chile) have been extensively studied in the past decade (e.g. Hubbard et al., 2010; Macauley and Hubbard, 2013; Hubbard et al., 2014; Pemberton et al., 2016; Reimchen et al., 2016; Daniels et al., 2018; Hubbard et al., 2020) and provide an excellent testing ground for the application of the SBE to an ancient deep-water depositional system. The challenge of applying the SBE to ancient systems is making the distinction between the dimensions of channel fill deposits and the dimensions of the conduit that define their sediment fluxes. Channel fill sandstones are commonly compound deposits formed by multiple turbidity currents during alternating phases of erosion and deposition. Thus channel dimensions associated with a single turbidity current are uncorrelated to those of the channel fills. Hubbard et al (2014; 2020) recognized this discrepancy and argued for using inter-channel erosion surfaces to make the distinction between sediment conduit dimensions (“storey” deposit) versus those of the composite channel element The analysis below will investigate the significance of this interpretation for the projected sediment budget associated with the lifespan of a channel element. Additionally, an erroneous attribution of channel complex dimensions, which are commonly observed in seismic data (Samuel et al., 2003; Macauley & Hubbard, 2013), to the characteristic turbidity current scale will be investigated.

Boundary Conditions

Channel form dimensions --- Channel form dimensions are estimated for the “M2” channel element, which is the focus of the recent paper by Hubbard et al. (2020). Three sets of dimensions are used as input conditions (Table Tres Pasos Scale): a) intra-channel element surfaces delineating channel storey deposits have vertical and horizontal scales of 2.5-6.5 m and ~200 m, respectively(Hubbard et al., 2020); b) the primary channel surface delineating the M2 channel element deposit has a vertical scale of 17 m, and is 400 m wide (Hubbard et al., 202X); and c) channel elements are commonly grouped in channel complexes that are typically 800-1000 m wide, and 30-60 m thick (Macauley and Hubbard, 2013).

System Slope --- The M2 channel is part of the Figueroa clinothem (*sensu* Hubbard et al., 2010), which has an estimated paleorelief of ~1000 m. Daniels et al. (2018) estimated the paleo-slope at this position in the Figueroa clinothem at 0.7-0.9°.

Grainsize --- The axial channel-fill deposits of the Tres Pasos Formation slope channels are dominated by amalgamated, thick bedded, fine to medium-grained sandstones. Grainsize measurements on thin section images yielded a D_{50} of 200 µm (de Leeuw, 2017). The D_{90} was measured as 400 µm.

Turbidity current duration --- Tres Pasos Formation contains relatively small, slope channels with a length of 10s of km, and the flow duration is therefore set to 3-6 hours.

Turbidity currents frequency and system activity --- Hubbard et al. (2020) recognized evidence for approximately 500 turbidity current events in the terrace deposits on the margin of the M2 channel. For the purpose of the parameterization of the SBE input conditions, this event count is transformed into paired values of decadal recurrence times and 5kyr system activity.

	Scenario Storey	Scenario Element	Scenario Complex
Channel Width [m]	200+/-10%	400+/-10%	800-1000
Channel Depth [m]	2.5-6.5	17+/-10%	30-60
System Slope [°]	0.7-0.9	0.7-0.9	0.7-0.9
Thalweg grainsize (d_{50}; d_{90}) [µm]	200;400	200;400	200;400
Sediment Concentration [%]	0.2-0.6	0.2-0.6	0.2-0.6
Current Duration [h]	3-6	3-6	3-6
Current Frequency [-/yr]	0.1	0. 1	0.1
System Activity [kyr]	5	5	5

Table 2: *Input conditions used to simulate characteristic turbidity currents at the storey, element, and complex scales in the Tres Pasos Formation.*

Results

From the constraints of the field data, the SBE model predicts turbidity current structure and the sediment flux and budget for the different stratigraphic scales of channel organization. We here follow the interpretation by Hubbard et al. (2014; 2020) that the intra-element surfaces that delineate channel storeys are correlated to the scale of the characteristic turbidity currents that formed the compound channel-element deposit. The structure of these characteristic turbidity currents at the channel-storey scale is therefore discussed in most detail before addressing the implications of using channel-element and channel-complex scales in estimating the systems sediment flux/budget.

Turbidity Current Structure --- Turbidity currents are simulated to flow at a maximum velocity of just over 1 m/s (Fig. 9a). The velocity maximum of the single simulation presented in this figure is located approximately 2 m above the bed, roughly half of the mean channel-storey surface elevation. The velocity decreases until it approximates 0 m/s at 10-12 m above the channel floor. The sediment concentration profile displays strong stratification, with most sediment suspended near the base of the flow (Fig. 9b). The basal sediment concentration of the example simulation is 2.5 % by volume, yet at the elevation of the maximum velocity (2 m), the sediment concentration has decreased to less than 0.1 % by volume. The mean of the basal sediment concentrations for all 2401 simulated characteristic turbidity currents is 3.0 % by volume, roughly 10 times the depth-averaged sediment concentration used as input condition (0.2-0.6 % vol.).

Sediment flux and budget --- The simulated sediment fluxes through the channel cross section are 0.9-2.5-5.8 m^3/s (p_{10}-p_{50}-p_{90}; Fig. 9c). This amounts to a sediment budget of $6.6*10^6$-$2.0*10^7$-$4.5*10^7$ m^3 (p_{10}-p_{50}-p_{90}) over the full evolution of the 500 turbidity currents that formed the channel-element deposit (Fig. 9d).

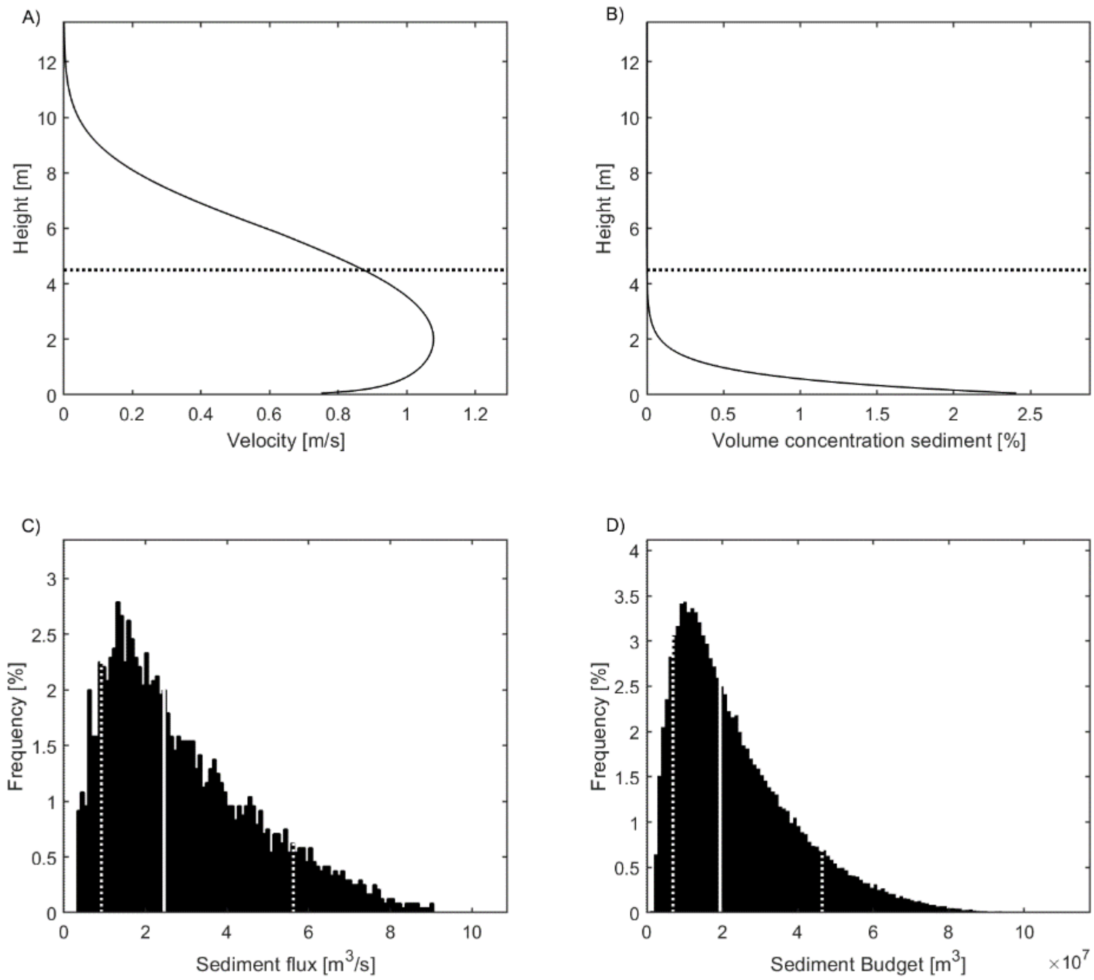

Fig. 9: *SBE-results for characteristic turbidity currents related to storey-dimensions in Tres Pasos Formation slope channels. A) Velocity profile of one typical simulation, dotted line indicates mean storey-surface depth. B) Sediment concentration profile of one typical simulation. C) Histogram of calculated sediment fluxes through the channel cross-section per second. Vertical white line indicates the p_{50} of predicted sediment flux, white dotted lines indicate p_{10} and p_{90}. D) Histogram of cumulative sediment budget of 500 characteristic turbidity currents. Vertical white line indicates the p_{50} of predicted sediment budgets, white dotted lines indicate p_{10} and p_{90}.*

Storey – element – complex --- The larger dimensions of the composite channel-element and channel-complex scales lead, if associated with characteristic turbidity currents, to much larger flows and sediment budgets (Fig. 10). The simulated flow velocities increase to 2.5 and 4 m/s, respectively (Fig. 10a). This combines with the much thicker column of suspended sediment to accumulate sediment budgets that are in the order of 10^8 m^3 for the element-dimension simulations and 10^9 m^3 (1 km^3) for the complex-dimensions simulations. Rather than the 10^7 m^3 simulated when storey dimensions are used to simulate the characteristic turbidity currents (Fig. 10b).

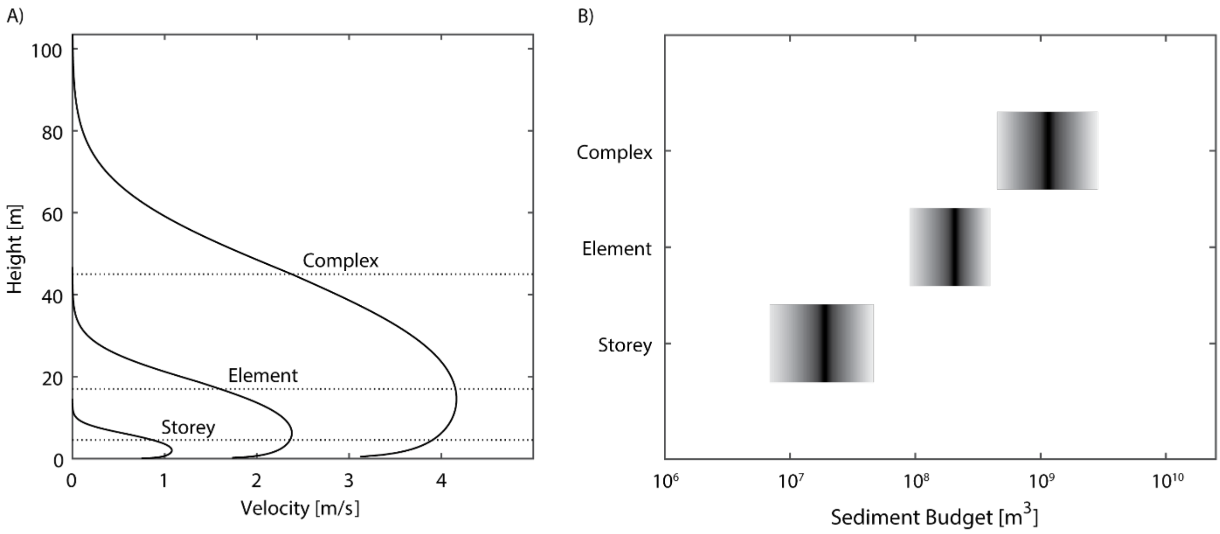

Fig. 10: A) Example characteristic turbidity currents resulting from storey dimensions, element dimensions, and complex dimensions.

Evaluation

Highly stratified turbidity current structure --- The majority of the sediment in the characteristic turbidity currents simulated for the Tres Pasos Formation M2 channel is suspended near the base of the flow. The remainder of what would typically be viewed as "the turbidity current" (say from 2-12 m above the bed), is relatively devoid of sediment. This result corroborates recently emerging measurements and perspectives on the concentration structure of turbidity currents. Measurements of sediment concentration with Acoustic Doppler Current Profilers (ADCPs) indicate that sediment concentrations in the bulk of the recorded flows are indeed very low (~0.02 %; Azpiroz-Zabala et al., 2017; Simmons et al., 2020). ADCPs have generally been deployed above submarine channels and canyons, to monitor turbidity currents downwards, which gives interference and resolution problems near the bed. These measurement difficulties mean that the 2 m thick part with elevated sediment concentrations depicted in Fig. 9b would typically be poorly resolved at most in ADCP data (Simmons et al., 2020). This would obscure the fact that the turbidity current is a very dilute cloud that is driven mainly by a dense basal layer (Cartigny et al., 2013; Paull et al., 2018; Simmons et al., 2020).

It is interesting to discuss here how stratification of concentration profiles is included in depth-averaged modelling workflows of turbidity currents, an approach that is more complicated than the simplified approach of the SBE. Parker (1982) proposed a simple measure for stratification in depth-averaged modelling of turbidity currents: the ratio between the near-bed sediment concentration and the depth-averaged sediment concentration, r_o, a notation that has mostly been followed by the many papers following the depth-averaged approach to modelling turbidity currents (for recent examples see Halsey et al., 2017; Bolla Pittaluga et al., 2018; Traer et al., 2018). On its first appearance, r_o was evaluated as a function of grain size with the Rouse equation for suspended sediment concentration (Parker, 1982). The Rouse equation was not derived for turbidity currents, but for open channel flow (Rouse, 1938). Even though it has been shown to be a reasonable approximation for fine grained suspended sand, and in general for the sediment suspended in the lower part of the flow, it mispredicts suspension of mud, especially in the upper part of the flow, because it neglects mixing with the ambient water in the mixing layer (Eggenhuisen et al., 2019). Parker et al. (1986) dropped reliance on the Rouse equation and instead advised a value of r_o=1.6, while Garcia (1994) advised r_o=2.0, both based on a compilation of concentration profiles obtained from weakly-stratified, small-scale laboratory experiments. These low values for r_o are used in modelling studies to this date (Traer *et al.*, 2012; Halsey *et al.*, 2017; Bolla Pittaluga *et al.*, 2018). Dorrell et al. (2014) attempted to validate depth-averaged simulations with unstratified “top-hat” concentration profiles (with r_o=1) and weakly-stratified profiles against measurements of gravity currents in the Black Sea. The unsatisfactory results of their validation led Dorrell et al. (2014) to hypothesize that field-scale flows have larger degrees of stratification that are poorly represented by the stratification observed in small scale experiments. Recent acoustic measurements of sediment concentrations in the Congo Canyon indicate that r_o was ~10 in the turbidity currents reported by Azpiroz-Zabala et al. (2017) and Simmons et al. (2020). The SBE results presented here are consistent with this elevated stratification in field-scale turbidity currents compared to laboratory turbidity currents, with r_o~10 for the Tres Pasos simulations, and r_o~11 for the Grand Banks simulation (Figs. Experiment, Tres Pasos, Grand Banks).

Sediment flux and budget of the M2 channel element --- The simulated sediment flux through the M2 channel (Fig. 9) is comparable to the sediment flux of the turbidity currents in the Congo Canyon reported by Azpiroz-Zabala et al. (2017). The total sediment budget of the M2 channel element is comparable to the "X-channel" on the Niger slope (1.7-5.2*10^7 m^3; Jobe et al., 2018), though this was delivered to the lobe by a smaller number (20-50) of turbidity currents with a centennial recurrence time, rather than the 500 events of the M2 channel. The M2 sediment budget is smaller than the volumes of other Quarternary fans evaluated in Jobe et al. (2018), which are typically order 10^9 km^3 with event counts varying from 10-700. This comparison shows that the reconstructed sediment flux and budget for the M2 channel are within the bandwidth of values measured in other systems, though on the lower part of this bandwidth. This is consistent with the suggestion by Jobe et al (2018) that smaller volumes are associated with intraslope and base-of-slope channels. A consideration of stratigraphic hierarchy could also explain the modest sediment budget predicted for the M2 channel element. Though it is not entirely clear whether lobe elements (Prélat *et al.*, 2009) can be correlated one-to-one with a single, coeval channel element (Cullis *et al.*, 2018), it is interesting to observe that the predicted sediment budget for the M2 channel compares very well with the volume estimates of lobe elements compiled by Prélat et al. (2010). This point will be considered further in the section below.

Storey – Element – Complex – Fan --- Constraining the SBE with different hierarchical scales leads to disparate distributions of predicted sediment budgets (Fig. 10). The p_{10}-p_{90} ranges of the 3 sets of simulations do not overlap. Each step upward in dimensions of the assumed contemporaneous channel form results in roughly an order of magnitude increase in predicted sediment budget. Hubbard et al. (2014; 2020) have argued extensively for the association between intra-channel element surfaces and formative turbidity current processes based on facies analyses. The larger channel-fill deposits recognized in single channel elements are formed by a compound evolution of erosion and deposition, akin to “the fluvial valleys that never were” of Strong and Paola (2008; Hubbard et al., 2020). Association of channel element thickness with formative turbidity current flows would lead to much thicker (17 m vs 2.5-6.5 m) and faster flow (~2.5 m/s vs. ~1 m/s), which combines to yield an order of magnitude larger sediment budget over the 500 turbidity currents constituting the lifespan of the M2 element. Multiple channel elements are commonly stacked consistently into channel complexes (e.g. McHargue et al., 2011; Macauley and Hubbard, 2013). In our preferred interpretation, the sediment budget for channel complexes is obtained by multiplying the budget based on intra-channel surfaces (channel storey dimensions) by the typical count of elements in a complex. Macauley and Hubbard (2013) mapped 18 channel elements in the three channel complexes that form the lower half of the Figueroa clinothem. This suggests a typical sediment budget during one channel complex evolution of ~$1*10^8$ m^3 (p_{50}), much less than the volumes predicted if the complexes themselves were erroneously associated with formative turbidity currents (p_{50}= $1.2*10^9$ m^3). This illustrates the consequences of erroneously relating channel fill or complex dimensions to the sizes of their formative flows. It also emphasizes that careful interpretation of stratigraphy matters a great deal for accurate estimation of primary aspects of the system, such as the order of magnitude of sand transported down-dip. This is particularly important in large-scale subsurface datasets that can lack resolution to map individual elements.

Extrapolation of the sediment budget to the entire sand-rich package of the Figueroa clinothem at the Laguna Figuaroa localities (Macauley and Hubbard, 2013; Hubbard et al., 2014; Pemberton et al., 2016; Hubbard et al., 2020) yields a total SBE-derived turbidity-current sediment budget of order 1 km^3. This volume would have been deposited during an unconstrained subsidiary phase within an ~ 2

Myr stratigraphic interval duration (Daniels et al., 2018). The depositional body formed at this largest timescale could appropriately be called a fan. This SBE volume estimate is an entry into the suite of source-to-sink metric correlations available from literature (Somme *et al.*, 2009b; a). A 1 km^3 volume for the Figueroa clinothem fan could correlate to a fan length of 20-150 km, and a fan area of order 1000 km^2 (Somme *et al.*, 2009b).

GENERAL DISCUSSION

An Extra Tool in the Source-to-Sink Toolshed

Estimations of sediment budgets in submarine depositional systems is interesting in its own right, but can also form an inroad into a broader understanding of the setting of the system in a source-to-sink analysis (Jobe et al., 2018). An important aspect of source-to-sink analyses is that metrics obtained for different segments can be correlated to each other because regional plate tectonic and climatic conditions ensure regulate consistency within a system (Somme *et al.*, 2009b; a; Walsh *et al.*, 2016). By predicting metrics of basin-floor lobes from base-of-slope channel metrics the SBE intrinsically correlates between the deep-marine segments of the chain of sediment transport. Furthermore, the reconstructed fan volume, length, and area can be used to estimate a correlated slope length (Somme *et al*., 2009a; 2009b). The estimated slope length for the Tres Pasos Formation example analysed above would be kilometers to tens of kilometers, which is consistent the stratigraphic reconstructions of Daniels et al. (2018). Dimensions of the shelf-staging area (Somme et al., 2009a) can be evaluated against the depositional style of coeval shelf-top delta deposits of the Dorotea Formation (Romans *et al.*, 2011; Daniels *et al.*, 2018). And correlated long-term deposition rates of order 10^6 t/yr (Somme *et al.*, 2009a) can be used to evaluate the nature of river catchment areas that supplied sediment from the Andes into the retro-arc foreland basin (Romans *et al.*, 2011).

Sediment budget estimations are a rapidly evolving topic in sedimentary system science. It has been developed for the sediment budget coming from continental catchment areas over decadal timescales in the BQART model (Syvitsky & Milliman, 2007; Somme *et al.*, 2011; Helland-hansen *et al.*, 2016), and for the geological sediment budget in fluvial systems using the fulcrum approach (Holbrook & Wanas, 2014; Bhattacharya *et al.*, 2016; Lin & Bhattacharya, 2017; Sharma *et al.*, 2017). The fulcrum method perceives a fluvial channel cross section as the pivot between the sediment load received from the up-stream domain and transmitted to a downstream domain. It analyzes the relation between local channel-fill deposit architecture and this expected sediment throughput. The SBE has a nearly identical philosophy to the fulcrum approach, but applied to submarine channel-cross sections. Indeed, the relation between channel deposit architecture and the formative turbidity current processes that were once active is critical in determining the sediment budgets (see section 6.3, above). Estimations with as many different tools as possible are combined in an ideal source-to-sink study. Where possible, triple assessments with BQART on catchment area budget, the fulcrum approach for the fluvial segment, and the SBE for the deep-marine segments will result in a consistency check that can confirm the source-to-sink understanding of a system. In this sense, the SBE should be regarded as a tool in the growing toolshed of source-to-sink studies.

Model functionality and complexity

Functionality --- The EuroSEDS-SBE is an example of simplified modelling where much of the hydraulic complexity is hidden from the intended users (marine and sedimentary geologists) because it could lie outside their immediate area of expertise. The simplicity of the tool presented here allows computation of 10^4 turbidity currents within seconds on a standard desktop computer. This makes the tool suited to consider multitudes of scenarios, resulting in the probability distribution function of sediment fluxes into the deep oceans. Also, its computational efficiency lends itself to running multiple simulations to test different geological perspectives, and the overall sensitivity of the system. The benefit of such a rapid interaction is that the geologist gains immediate insight into the consequence of different geological models for the probability distribution of predicted sediment budgets. There is no overstating of the importance of sensible geological interpretations of the stratigraphic observations of a system. The Tres Pasos Formation evaluation shows that interpretations of stratigraphic hierarchy are a primary control the scale of sediment budget estimations. An even more fundamental point is made here by comparing budget histograms of simulations with different uncertainty bounds (Table 3). The middle scenario represents the base case used earlier to evaluate the basic structure of the SBE results and perform a sensitivity analysis. The minimum and maximum bounds of ranges of input conditions were set to differ by a factor of 2-3 in that scenario. This resulted in a log-normal distribution of estimated sediment budgets (Figs. 3d & 11b). An over-confident geologist may ascertain uncertainty bounds of +/-10 %, which is normally only possible under controlled laboratory conditions or in modern systems with high-fidelity monitoring. This over-confidence leads to sediment budget predictions that approaches a normal distribution, closely centered around the p_{50} (Fig. 11a). Finally, a scenario with broad uncertainty (a factor 5 difference between minimum and maximum input conditions) results in an exponential distribution with the highest probability being that the sediment budget is small, but very large values also considered a possibility (Fig. 11c). These results demonstrate that the degree of geological uncertainty is directly linked to the shape of the Probability Density Function (PDF) of the system's sediment-budget estimations. It is worth noting that the shape of these PDFs are not discrete, but transition into each other with growing levels of uncertainty. This implies that the distributions are in fact all realizations of a single family of PDFs such as the binomial function or Poisson function, which are two and one-parameter functions respectively. The premise is then that it should be possible to parameterize the distribution of sediment budgets directly from the boundary conditions, without the need of the Monte Carlo realizations of the SBE. This mathematical exercise is not pursued herein.

As an ultimate test of geological uncertainty, a simulation was run with input parameters set to minimum and maximum values that cover most of the submarine literature. The resulting predictions of sediment budgets were, perhaps unsurprisingly, that any amount of sediment might have gone through these channels, yet that the most likely amount converges to nothing. Process-based prediction of sediment budget is thus not possible in absence of geological constraints on the model. This insight justifies continued efforts by the sedimentological community to try to understand the expression of turbidity current processes in the stratigraphic record. It also underscores the need for modelers and stratigraphers to engage in integrated projects. This should motivate the research community to strive for integrated studies with research teams involving both experts in stratigraphy and sediment transport processes.

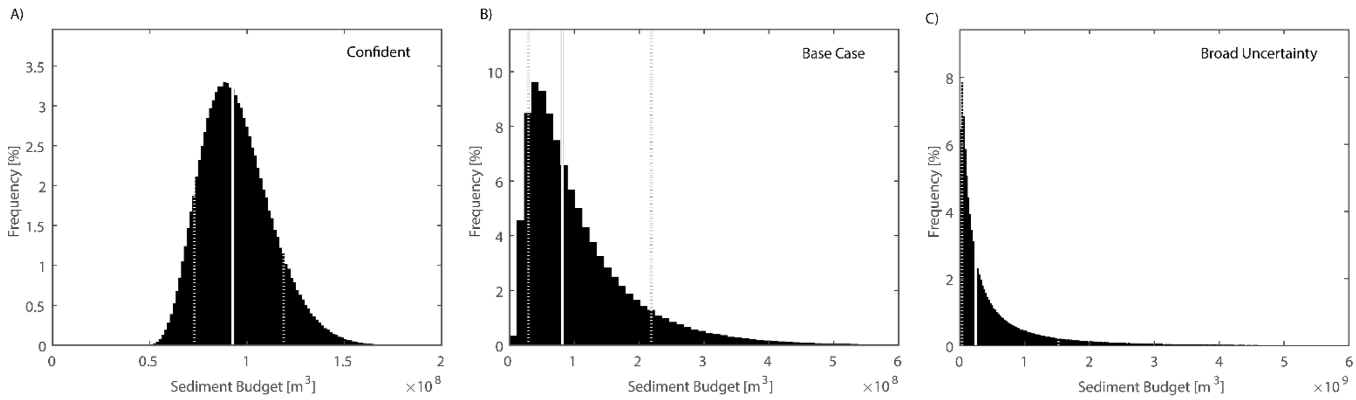

Fig. 11: *Sediment budget histograms for scenarios with decreasing confidence of interpretation. Vertical white line indicates the p_{50} of predicted sediment budgets, white dotted lines indicate p_{10} and p_{90}. A) Confident levels of uncertainty with +/-10% ranges around a mean estimates of input conditions. B) The base case scenario with factor 2-3 differences between minimum and maximum inputs. C) Broad uncertainty with a factor 5 difference between minimum and maximum inputs.*

	Scenario Confident	Scenario Base Case	Scenario Broad Uncertainty
Channel Width [m]	300 +/-10%	200-400	100-500
Channel Depth [m]	15 +/-10%	10-20	6-30
System Slope [°]	1.75 +/-10%	1-2.5	0.5-2.5
Thalweg grainsize (d_{50}; d_{90}) [µm]	150; 350	150; 350	150; 350
Sediment Concentration [%]	0.4 +/-10%	0.2-0.6	0.2-1.0
Current Duration [h]	3 +/-10%	2-4	2-10
Current Frequency [-/yr]	0.075 +/-10%	0.05-0.1	0. 03-0.15
System Activity [kyr]	7.5 +/-10%	5-10	2-10

Table 3: *The input conditions used to illustrate the effect of scenario confidence on predicted downdip sediment volumes.*

Complexity --- While the SBE results are consistent with known cases at the largest and smallest scales, the simulated flow structures in fact differ for the different scales (Fig. 6 vs. 7 & 9). Specifically, the real world flows are more stratified at their base, meaning that the near-bed gradients in suspended sediment concentration are larger in nature than in small scale laboratory experiments. Another striking feature is that the SBE captures the similarity of scale in flow velocity between real world (Tres Pasos) and experimental flows (order 1 m/s), despite the 2 orders of magnitude difference in flow thickness. The fact that the SBE produces varying turbidity current structures at varying scales is a sign that while it is a simple model, it is still complex enough to yield results that cannot be foreseen and that fulfill the essential requirement of any model: we can learn something new about the process from the model results.

Empirical relations obtained by fitting small-scale experimental data cannot readily be extrapolated to full field scale, because there is always the concern of extrapolating beyond the parameter space for which the relation was originally obtained. Understanding of the physical processes, however, can be based on small scale experiments, because the equations that describe the physical process can yield different predictions at different scales. This is illustrated by the ability of the SBE to simulate strongly stratified, high-r_o turbidity currents at field scale while many of the ideas were justified from scientific studies of small scale experiments with poorly stratified flows. It further demonstrates that the aim of an experimental study in sedimentology can, and should be to learn more about nature, not to learn more about the laboratory. We suggest that researchers modelling turbidity currents at the full natural scale consider highly stratified flows with r_o~10, in future work, rather than the customary weakly stratified values of 1.6-2.0. Better still, since the input conditions of the SBE are a limited subset of the boundary conditions required for depth-averaged modelling of turbidity currents, such models could *a priori* query the SBE to obtain an estimate for r_o. These considerations are an illustration of how more simple models can be used to direct more complex models to more relevant segments of their parameter space, and how model integration between simple and more complex models can improve the relevance of simulations performed.

More complex modelling workflows exist for turbidity-current research that addresses questions beyond bulk sediment budgets. It is tempting to select one of these more complex approaches in the pursuit of higher-fidelity results. However, a potential pitfall is that more intricate model systems are in practice associated with more parameters and variables and will therefore require the user to set more intricate and precise boundary conditions, i.e. to be more knowledgeable about the system *a priori*. This is a problem especially in ancient systems, where parameters such as bathymetry can have a controlling effect on modelled turbidity currents, yet are essentially unresolved at the resolution needed for high-fidelity simulations (Aas *et al.*, 2010). The model presented in this paper has purposefully been designed with many simplifications, so that it can serve as the first, quick, check of a system's range of parameters, either as the final stage in sediment budget estimation workflows, or ahead of more concerted modelling efforts with higher-fidelity modelling approaches. The benefits of the simplified modeling approach of the SBE that have been emphasized in this discussion do not preclude meaningful future extensions of the model. One desirable extension could be to include physics-based modelling of the concentration profile, the shape of which is now included with a crude exponential equation; another is the incorporation of grain-size distributions within the concentration profiles. Another useful added complexity could be distinction between flow structure and sediment flux in short duration, dense, thin, fast, frontal cells and extended (in time), dilute, quasi-steady phases that have recently been described in monitoring studies (Azpiroz-Zabala et al., 2017; Simmons et al., 2020; Wang et al., 2020). These different phases of events could have different roles in the sediment fluxes along deep-marins systems, while the initial version of the SBE presented here assumes a single, steady flow structure during the entire event duration. Such extensions of the SBE, however, should not come at the expense of the core virtues of the SBE as called for by Somme and Martinsen (2017): a simple, quantitative model, which reflects natural variability and can be applied to ancient systems.

CONCLUSIONS

We presented the Sediment Budget Estimator, a simplified, robust model that links the flow structure of turbidity currents to observable submarine channel characteristics. The SBE uses this structure for stochastic first order predictions of sediment fluxes and budgets in channelized turbidity current systems. The model has been structured such that all necessary input conditions can be obtained from geological or oceanographic observations or published analogue datasets. A sensitivity analysis reveals that fundamental uncertainty about the sediment concentration of turbidity currents has the largest impact on variability of the results. Channel width also has a marked effect. Aspects of timing of turbidity currents (recurrence time, duration of individual flows, and duration of the geological activity of the system) all have linear influences on uncertainty.

Channel depth is less influential and the slope of the system has a surprisingly modest effect on the results.

The SBE is successfully validated against small scale laboratory experiments and the 1929 Grand Banks turbidity current, with sediment budgets that differ by 12 orders of magnitude.

Application of the model to slope-channel deposits of the Cretaceous Tres Pasos Formation demonstrates the potential for paleo sediment-budget estimations. Intra channel-deposit surfaces with a vertical amplitude of 2.5-6.5 m are associated with formative turbidity currents. Alternative, less likely, associations between formative currents and channel element or channel complex scales yield budget estimates that are 1 or 2 orders of magnitude too large, respectively. The estimates of sediment budget for the lifespan of a single channel element offer an inroad into estimation of lobe element, lobe, and fan volumes. These can in turn be correlated to metrics of the slope, shelf, and catchment segments of the source-to-sink system. In such a comprehensive source to sink analysis the SBE can be applied in tandem with existing sediment budget estimators for catchment areas and fluvial systems, such as BQART and the Fulcrum approach for fluvial paleohydrology. As such, the SBE represents a new tool in the growing toolshed of source-to-sink studies of sedimentary systems.

Application of the SBE to submarine channels and their deposits in modern sea-floor settings, geological outcrops of ancient systems, and subsurface datasets will enable first order flux and budget predictions and reconstructions of sediment and other phases.

SUPPORTING MATERIAL

The Matlab scripts that constitute the Eurotank Studies of Experimental Deepwater Sedimentology Sediment Budget Estimator (EuroSEDS-SBE) will be made available as supplementary material to this paper on publication.

ACKNOWLEDGMENTS

JTE, MT, FP, JdL, and YS acknowlegde funding of the EuroSEDS project by NWO (grant #), ExxonMobil, Shell, and Equinor.

Discussions with Michal Janocko helped direct the functionality of the SBE at an early stage.

The participants of the Utrecht University MSc course Dynamics of Sedimentary Systems (2018-2020) are gratefully acknowledged for testing the SBE. Their course work pointed out the bugs and benefits of the SBE. Their collective success in using the SBE to constrain sediment budgets in diverse deep-water systems has provided the necessary motivation to carry this manuscript to completion.

REFERENCES

Aas, T.E., **Howell, J.A.**, **Janocko, M.** and **Jackson, C.A.L.** (2010) Control of Aptian palaeobathymetry on turbidite distribution in the Buchan Graben, Outer Moray Firth, Central North Sea. *Mar. Pet. Geol.*, **27**, 412–434.

Abd El-Gawad, S., **Cantelli, A.**, **Pirmez, C.**, **Minisini, D.**, **Sylvester, Z.** and **Imran, J.** (2012) Three-dimensional numerical simulation of turbidity currents in a submarine channel on the seafloor of the Niger Delta slope. *J. Geophys. Res.*, **117**, C05026.

Allin, J.R., **Hunt, J.E.**, **Clare, M.A.** and **Talling, P.J.** (2018) Eustatic sea-level controls on the flushing of a shelf-incising submarine canyon. *GSA Bull.*, 222–237.

Altinakar, M.S., **Graf, W.H.** and **Hopfinger, E.J.** (1996) Flow structure in turbidity currents. *J. Hydraul. Res.*, **34**, 713–718.

Amblas, D., **Canals, M.**, **Urgeles, R.**, **Lastras, G.**, **Liquete, C.**, **Hughes-Clarke, J.E.**, **Casamor, J.L.** and **Calafat, A.M.** (2006) Morphogenetic mesoscale analysis of the northeastern Iberian margin, NW Mediterranean Basin. *Mar. Geol.*, **234**, 3–20.

Arfaie, A., **Burns, A.D.**, **Dorrell, R.M.**, **Eggenhuisen, J.T.**, **Ingham, D.B.** and **McCaffrey, W.D.** (2014) Optimised mixing and flow resistance during shear flow over a rib roughened boundary. Int Commun Heat Mass Transf. doi: 10.1016/j.icheatmasstransfer.2014.08.005

Azpiroz-zabala, M., **Cartigny, M.J.B.**, **Talling, P.J.**, **Parsons, D.R.**, **Sumner, E.J.**, **Clare, M.A.**, **Simmons, S.M.**, **Cooper, C.** and **Pope, E.L.** (2017) Newly recognized turbidity current structure can explain prolonged flushing of submarine canyons. *Sci. Adv.*, **3**, e1700200.

Azpiroz-Zabala, M., **Cartigny, M.J.B.**, **Talling, P.J.**, **Parsons, D.R.**, **Sumner, E.J.**, **Clare, M.A.**, **Simmons, S.M.**, **Cooper, C.** and **Pope, E.L.** (2017) Newly recognized turbidity current structure can explain prolonged flushing of submarine canyons. *Sci. Adv.*, **3**, e1700200.

Baas, J.H., **McCaffrey, W.D.** and **Knipe, R.J.** (2005) The Deep-Water Architecture Knowledge Base : towards an objective comparison of deep-marine sedimentary systems. *Pet. Geosci.*, **11**, 309–320.

Basani, R., **Janocko, M.**, **Cartigny, M.J.B.**, **Hansen, W.M.** and **Eggenhuisen, J.T.** (2014) MassFLOW-3D TM as a simulation tool for turbidity currents : some preliminary results. *IAS Speical Publ.*, **46**, 587–608.

Beelen, D., **Jackson, C.A.L.**, **Patruno, S.**, **Hodgson, D.M.** and **Alexandre, J.P.T.** (2019) The effects of differential compaction on clinothem geometries and shelf-edge trajectories. *Geology*, **47**, 1011–1014.

Best, J.L., **Kirkbride, A.D.** and **Peakall, J.** (2001) Mean flow and turbulence structure of sediment-laden gravity currents: new insights using ultrasonic Doppler velocity profiling. Spec. Publ. IAS 159–172.

Bhattacharya, J.P., **Copeland, P.**, **Lawton, T.F.** and **Holbrook, J.** (2016) Earth-Science Reviews Estimation of source area , river paleo-discharge , paleoslope , and sediment budgets of linked deep-time depositional systems and implications for hydrocarbon potential. *Earth Sci. Rev.*, **153**, 77–110.

Bolla Pittaluga, M., **Frascati, A.** and **Falivene, O.** (2018) A Gradually Varied Approach to Model Turbidity Currents in Submarine Channels. *J. Geophys. Res. Earth Surf.*, **123**, 80–96.

Cantero, M.I., **Balachandar, S.** and **Parker, G.** (2009) Direct numerical simulation of stratification effects in a sediment- laden turbulent channel flow. *J. Turbul.*, **10**, 37–41.

Cantero, M.I., **Cantelli, A.**, **Pirmez, C.**, **Balachandar, S.**, **Mohrig, D.**, **Hickson, T.A.**, **Yeh, T.**, **Naruse, H.** and **Parker, G.** (2011) Emplacement of massive turbidites linked to extinction of turbulence in turbidity currents. *Nat. Geosci.*, **5**, 42–45.

Cantero, M.I., **Shringarpure, M.** and **Balachandar, S.** (2012) Towards a universal criteria for turbulence suppression in dilute turbidity currents with non-cohesive sediments. *Geophys. Res. Lett.*, **39**, L14603.

Cartigny, M.J.B., **Eggenhuisen, J.T.**, **Hansen, E.W.M.** and **Postma, G.** (2013) Concentration-dependent flow stratification in experimental high-density turbidity currents and their relevance to turbidite facies models. *J. Sediment. Res.*, **83**, 1047–1065.

Champagne, F.H., **Pao, Y.H.** and **Wygnanski, I.J.** (1976) On the two-dimensional mixing region. *J. Fluid Mech.*, **74**, 209–250.

Chang, H.H. (1988) Fluvial processes in river engineering. *Krieger*, Malabar, FL, 446 pp.

Choux, C.M.A., **Baas, J.H.**, **McCaffrey, W.D.** and **Haughton, P.D.W.** (2005) Comparison of spatio–temporal evolution of experimental particulate gravity flows at two different initial concentrations, based on velocity, grain size and density data. *Sediment. Geol.*, **179**, 49–69.

Clare, M.A., **Hughes Clarke, J.E.**, **Talling, P.J.**, **Cartigny, M.J.B.** and **Pratomo, D.G.** (2016) Preconditioning and triggering of offshore slope failures and turbidity currents revealed by most detailed monitoring yet at a fjord-head delta. *Earth Planet. Sci. Lett.*, **450**, 208–220.

Clare, M.A., **Talling, P.J.**, **Challenor, P.**, **Malgesini, G.** and **Hunt, J.** (2014) Distal turbidites reveal a common distribution for large (>0.1 km3) submarine landslide recurrence. *Geology*, 263–266.

Clarke, J.E.H. (2016) First wide-angle view of channelized turbidity currents links migrating cyclic steps to flow characteristics. *Nat. Commun.*, **7**, 11896.

Cooper, C. (2013) Turbidity Current Measurements in the Congo Canyon. *Offshore Technol. Conf.*, 23992.

Covault, J.A., **Fildani, A.**, **Romans, B.W.** and **McHargue, T.** (2011) The natural range of submarine canyon-and-channel longitudinal profiles. *Geosphere*, **7**, 313–332.

Covault, J.A., **Normark, W.R.**, **Romans, B.W.** and **Graham, S.A.** (2007) Highstand fans in the California borderland: The overlooked deep-water depositional systems. *Geology*, **35**, 783–786.

Cullis, S., **Colombera, L.**, **Patacci, M.** and **McCaffrey, W.D.** (2018) Hierarchical classifications of the sedimentary architecture of deep-marine depositional systems. *Earth-Science Rev.*, **179**, 38–71.

Cullis, S., **Patacci, M.**, **Colombera, L.**, **Bührig, L.** and **McCaffrey, W.D.** (2019) A database solution for the quantitative characterisation and comparison of deep-marine siliciclastic depositional systems. *Mar. Pet. Geol.*, **102**, 321–339.

Daly, R.A. (1936) Origin of Submarine "Canyons." Am. J. Sci. 31:401–420.

Daniels, B.G., **Auchter, N.C.**, **Hubbard, S.M.**, **Romans, B.W.**, **Matthews, W.A.** and **Stright, L.** (2018) Timing of deep-water slope evolution constrained by large-n detrital and volcanic ash zircon geochronology, Cretaceous Magallanes Basin, Chile. *Bull. Geol. Soc. Am.*, **130**, 438–454.

Dorrell, R.M., **Darby, S.E.**, **Peakall, J.**, **Sumner, E.J.**, **Parsons, D.R.** and **Wynn, R.B.** (2014) The critical role of stratification in submarine channels: Implications for channelization and long runout of flows. *J. Geophys. Res. Ocean.*, **119**, 2620–2641.

Eggenhuisen, J.T., **Cartigny, M.J.B.** and **de Leeuw, J.** (2017) Physical theory for near-bed turbulent particle suspension capacity. *Earth Surf. Dyn.*, **5**, 269–281.

Eggenhuisen, J.T. and **McCaffrey, W.D.** (2012) The vertical turbulence structure of experimental turbidity currents encountering basal obstructions: implications for vertical suspended sediment distribution in non-equilibrium currents. *Sedimentology*, **59**, 1101–1120.

Eggenhuisen, J.T., **Tilston, M.C.**, **Leeuw, J.**, **Pohl, F.** and **Cartigny, M.J.B.** (2019) Turbulent diffusion modelling of sediment in turbidity currents: An experimental validation of the Rouse approach. *Depos. Rec.*, 203–216.

Garcia, M. and **Parker, G.** (1993) Experiments on the entrainment of sediment into suspension by a dense bottom current. *J. Geophys. Res.*, **98**, 4793–4807.

Garcia, M. and **Parker, G.** (1989) Experiments on hydraulic jumps in turbidity currents near a canyon-fan transition. *Science*, **245**, 393–396.

Garcia, M.H. (1994) Depositional turbidity currents laden with poorly sorted sediment. *J. Hydraul. Eng.*, **120**, 1240–1263.

García, M.H. (2008) Sedimentation engineering. *the American Society of Civil Engineers*, Rseton, Virginia, 1132 pp.

Gray, T.E., **Alexander, J.** and **Leeder, M.R.** (2005) Quantifying velocity and turbulence structure in depositing sustained turbidity currents across breaks in slope. *Sedimentology*, **52**, 467–488.

Halsey, T.C., **Kumar, A.** and **Perillo, M.M.** (2017) Journal of Geophysical Research : Oceans Depth-averaged theory. *J. Geophys. Res. Ocean.*, 1–26.

Hamilton, P., **Gaillot, G.**, **Strom, K.**, **Fedele, J.** and **Hoyal, D.** (2017) Linking hydraulic properties in supercritical submarine distributary channels to depositional-lobe geometry. *J. Sediment. Res.*, **87**, 935–950.

Heerema, C.J., **Talling, P.J.**, **Cartigny, M.J.**, **Paull, C.K.**, **Bailey, L.**, **Simmons, S.M.**, **Parsons, D.R.**, **Clare, M.A.**, **Gwiazda, R.**, **Lundsten, E.**, **Anderson, K.**, **Maier, K.L.**, **Xu, J.P.**, **Sumner, E.J.**, **Rosenberger, K.**, **Gales, J.**, **McGann, M.**, **Carter, L.** and **Pope, E.** (2020) What determines the downstream evolution of turbidity currents? *Earth Planet. Sci. Lett.*, **532**, 116023.

Heezen, B.C. and **Ewing, M.** (1952) Turbidity currents and submarine slumps, and the 1929 Grand Banks earthquake. *Am. J. Sci.*, **250**, 849–873.

Helland-Hansen, W., **Sømme, T.O.R.O.**, **Martinsen, O.L.E.J.**, **Lunt, I.A.N.** and **Thurmond, J.** (2016) DECIPHERING EARTH ’ S NATURAL HOURGLASSES : PERSPECTIVES ON SOURCE-TO-SINK ANALYSIS. 1008–1033.

Hermidas, N., **Eggenhuisen, J.T.**, **Jacinto, R.S.**, **Luthi, S.M.**, **Toth, F.** and **Pohl, F.** (2018) A Classification of Clay-Rich Subaqueous Density Flow Structures. *J. Geophys. Res. Earth Surf.*, **123**, 945–966.

Hizzett, J.L., **Hughes Clarke, J.E.**, **Sumner, E.J.**, **Cartigny, M.J.B.**, **Talling, P.J.** and **Clare, M.A.** (2018) Which Triggers Produce the Most Erosive, Frequent, and Longest Runout Turbidity Currents on Deltas? *Geophys. Res. Lett.*, **45**, 855–863.

Holbrook, J. and **Wanas, H.** (2014) A FULCRUM APPROACH TO ASSESSING SOURCE-TO-SINK MASS BALANCE USING CHANNEL PALEOHYDROLOGIC PARAMATERS DERIVABLE FROM COMMON FLUVIAL DATA SETS WITH AN EXAMPLE FROM THE CRETACEOUS OF EGYPT. *J. Sediment. Res.*, **84**, 349–372.

Hubbard, S.M., **Covault, J.A.**, **Fildani, A.** and **Romans, B.W.** (2014) Sediment transfer and deposition in slope channels: Deciphering the record of enigmatic deep-sea processes from outcrop. *Geol. Soc. Am. Bull.*, **126**, 857–871.

Hubbard, S.M., **Fildani, A.**, **Romans, B.W.**, **Covault, J.A.** and **McHargue, T.R.** (2010) High-Relief Slope Clinoform Development: Insights from Outcrop, Magallanes Basin, Chile. *J. Sediment. Res.*, **80**, 357–375.

Hughes Clark, J.E., **Shor, A.N.**, **Piper, D.J.W.** and **Mayer, L.A.** (1990) Large-scale current-induced erosion and deposition in the path of the 1929 Grand Banks turbidity current. *Sedimentologyimentology*, **37**, 613–629.

Islam, M.A. and **Imran, J.** (2010) Vertical structure of continuous release saline and turbidity currents. *J. Geophys. Res.*, **115**, C08025.

Jobe, Z., **Sylvester, Z.**, **Bolla Pittaluga, M.**, **Frascati, A.**, **Pirmez, C.**, **Minisini, D.**, **Howes, N.** and **Cantelli, A.** (2017) Facies architecture of submarine channel deposits on the western Niger Delta slope: Implications for grain-size and density stratification in turbidity currents. *J. Geophys. Res. Earth Surf.*, **122**, 473–491.

Jobe, Z.R., **Howes, N.**, **Romans, B.W.** and **Covault, J.A.** (2018) Volume and recurrence of submarine-fan-building turbidity currents. *Depos. Rec.*, **4**, 160–176.

Johannessen, E.P. and **Steel, R.J.** (2005) Shelf-margin clinoforms and prediction of deepwater sands. *Basin Res.*, **17**, 521–550.

Kane, I.A., **Ponten, A.S.M.**, **Vangdal, B.**, **Eggenhuisen, J.T.**, **Hodgson, D.M.** and **Spychala, Y.T.** (2017) The stratigraphic record and processes of turbidity current transformation across deep-marine lobes. *Sedimentology*, **64**, 1236–1273.

Khripounoff, A., **Vangriesheim, A.**, **Babonneau, N.**, **Crassous, P.**, **Dennielou, B.** and **Savoye, B.** (2003) Direct observation of intense turbidity current activity in the Zaire submarine valley at 4000 m water depth. *Mar. Geol.*, **194**, 151–158.

Kneller, B. (2003) The influence of flow parameters on turbidite slope channel architecture. *Mar. Pet. Geol.*, **20**, 901–910.

Kneller, B. and **Buckee, C.** (2000) The structure and fluid mechanics of turbidity currents: a review of some recent studies and their geological implications. *Sedimentology*, **47**, 62–94.

Kneller, B., **Nasr-Azadani, M.M.**, **Radhakrishnan, S.** and **Meiburg, E.** (2016) Long-range sediment transport in the world's oceans by stably stratified turbidity currents. *J. Geophys. Res. Ocean.*, 8608–8620.

Kneller, B.C., **Bennett, S.J.** and **McCaffrey, W.D.** (1999) Velocity structure, turbulence and fluid stresses in experimental gravity currents. *J. Geophys. Res.*, **104**, 5381.

Konsoer, K., **Zinger, J.** and **Parker, G.** (2013) Bankfull hydraulic geometry of submarine channels created by turbidity currents : Relations between bankfull channel characteristics and formative flow discharge. **118**, 216–228.

Krastel, S., **Braeunig, A.**, **Feldens, P.**, **Georgiopoulou, A.**, **Jaehmlich, H.**, **Lange, M.**, **Lindhorst, K.**, **Llopart, J.**, **Mader, S.**, **Mehringer, L.**, **Merl, M.**, **Muecke, I.**, **Renkl, C.**, **Roskoden, R.**, **M, S.**, **Schulten, I.**, **Scharwz, J.-P.**, **Stevenson, C.**, **Vallee, M.**, **Wegener, B.** and **Wiesenberg, L.** (2016) Geomorphology, processes and geohazards of giant submarine landslides and tsunami generation capacity, as recorded in the sedimentary record of the only historic slide of this kind: the 1929 Grand Banks landslide of the Canadian Atlantic continental margi. *MARIA S. MERIAN-Berichte*, **MSM47**, 55.

Kuenen, P.H. (1952) Estimated size of the Grand Banks turbidity current. *Am. J. Sci.*, **250**, 874–884.

Lastras, G., **Canals, M.**, **Amblas, D.**, **Lavoie, C.**, **Church, I.**, **De Mol, B.**, **Duran, R.**, **Calafat, A.M.**, **Hughes-Clarke, J.E.**, **Smith, C.J.** and **Heussner, S.** (2011) Understanding sediment dynamics of two large submarine valleys from seafloor data: Blanes and La Fonera canyons, northwestern

Mediterranean Sea. *Mar. Geol.*, **280**, 20–39.

Lee, S.E., **Talling, P.J.**, **Ernst, G.G.J.** and **Hogg, A.J.** (2002) Occurrence and origin of submarine plunge pools at the base of the US continental slope. *Mar. Geol.*, **185**, 363–377.

de Leeuw, J., **Eggenhuisen, J.T.** and **Cartigny, M.J.B.** (2016) Morphodynamics of submarine channel inception revealed by new experimental approach. *Nat. Commun.*, **7**, 10886.

de Leeuw, J. (2017) The sedimentary record of submarine channel morphodynamics. Utrecht University

de Leeuw, J., **Eggenhuisen, J.T.** and **Cartigny, M.J.B.** (2018a) Linking submarine channel–levee facies and architecture to flow structure of turbidity currents: insights from flume tank experiments. *Sedimentology*, **65**, 931–951.

de Leeuw, J., **Eggenhuisen, J.T.**, **Spychala, Y.T.**, **Heijnen, M.S.**, **Pohl, F.** and **Cartigny, M.J.B.** (2018b) Sediment volume and grain-size partitioning between submarine channel-levee systems and lobes: an experimental study. *J. Sediment. Res.*, **88**, 777–794.

Leopold, L.B. and **Maddock, T.J.** (1953) The hydraulic geometry of stream channels and some physiographic implications.

Lin, W.E.N. and **Bhattacharya, J.P.** (2017) ESTIMATION OF SOURCE-TO-SINK MASS BALANCE BY A FULCRUM APPROACH USING CHANNEL PALEOHYDROLOGIC PARAMETERS OF THE CRETACEOUS DUNVEGAN FORMATION , CANADA Alloformation in the Western Canadian Sedimentary Basin to test the total mass-balance fulcrum approach. *J. Sediment. Res.*, **87**, 97–116.

Macauley, R. V. and **Hubbard, S.M.** (2013) Slope channel sedimentary processes and stratigraphic stacking, Cretaceous Tres Pasos Formation slope system, Chilean Patagonia. *Mar. Pet. Geol.*, **41**, 146–162.

McHargue, T., **Pyrcz, M.J.**, **Sullivan, M.D.**, **Clark, J.D.**, **Fildani, A.**, **Romans, B.W.**, **Covault, J.A.**, **Levy, M.**, **Posamentier, H.W.** and **Drinkwater, N.J.** (2011) Architecture of turbidite channel systems on the continental slope: Patterns and predictions. *Mar. Pet. Geol.*, **28**, 728–743.

Middleton, G. V (1966) Small-scale models of turbidity currents and the criterion for auto-suspension. *J. Sediment. Petrol.*, **36**, 202–208.

Middleton, G. V (1993) Sediment deposition from turbidity currents. *Annu. Rev. Earth Planet. Sci.*, **21**, 89–114.

Mohrig, D. and **Buttles, J.** (2007) Deep turbidity currents in shallow channels. *Geology*, **35**, 155.

Mulder, T., **Savoye, B.**, **Piper, D.J.W.** and **Syvitski, J.P.M.** (1998) The Var submarine sedimentary system: understanding Holocene sediment delivery processes and their importance to the geological record. *Geol. Soc. Spec. Publ.*, **129**, 145–166.

Paola, C. and **Martin, J.M.** (2012) Mass-Balance Effects In Depositional Systems. *J. Sediment. Res.*, **82**, 435–450.

Parker, G., **Fukushima, Y.** and **Pantin, H.M.** (1986) Self-accelerating turbidity currents. *J. Fluid Mech.*, **171**, 145–181.

Parker, G., **Garcia, M.**, **Fukushima, Y.** and **Yu, W.** (1987) Experiments on turbidity currents over an erodible bed. *J. Hydraul. Res.*, **25**, 123–147.

Patruno, S., **Hampson, G.J.** and **Jackson, C.A.L.** (2015) Quantitative characterisation of deltaic and subaqueous clinoforms. *Earth-Science Rev.*, **142**, 79–119.

Patruno, S. and **Helland-Hansen, W.** (2018) Clinoform systems: Review and dynamic classification scheme for shorelines, subaqueous deltas, shelf edges and continental margins. *Earth-Science Rev.*, **185**, 202–233.

Piper, D.J.W. and **Aksu, A.E.** (1987) The source and origin of the 1929 Grand Banks turbidity current inferred from sediment budgets. *Geo-Marine Lett.*, **7**, 177–182.

Piper, D.J.W. and **Deptuck, M.** (1997) Fine-graines turbidites of the Amazon Fan: facies characterization and interpretation. *Proc. Ocean Drill. Porgram, Sci. Results*, **155**, 79–108.

Piper, D.J.W., **Shor, A.N.** and **Hughes Clark, J.E.** (1988) The 1929 Grand Banks earthquake, slump, and turbidity current. *GSA Spec. Pap.*, **229**, 77–92.

Pirmez, C. and **Imran, J.** (2003) Reconstruction of turbidity currents in Amazon Channel. *Mar. Pet.*

Geol., **20**, 823–849.

Pirmez, C., **Prather, B.E.**, **Mallarino, G.**, **O'Hayer, W.W.**, **Droxler, a. W.** and **Winker, C.D.** (2012) Chronostratigraphy of the Brazos–Trinity Depositional System, Western Gulf of Mexico: Implications for Deepwater Depositional Models. 111–143 pp.

Pittaluga, M.B. and **Imran, J.** (2014) Journal of Geophysical Research : Earth Surface A simple model for vertical profiles of velocity and suspended sediment concentration in straight and curved. 483–503.

Plapp, J.E. and **Mitchell, J.P.** (1960) A hydrodynamic theory of turbidity currents. *J. Geophys. Res.*, **65**, 983–992.

Pohl, F., **Eggenhuisen, J.T.**, **Cartigny, M.J.B.**, **Tilston, M.** and **Leeuw, J.** (2020) The influence of a slope break on turbidite deposits: an experimental investigation. *Mar. Geol.*, 1–33.

Pope, E.L., **Talling, P.J.**, **Carter, L.**, **Clare, M.A.** and **Hunt, J.E.** (2017) Damaging sediment density flows triggered by tropical cyclones. *Earth Planet. Sci. Lett.*, **458**, 161–169.

Pope, S.B. (2000) Turbulent Flows. *Cambridge University Press*, Cambridge, UK, 771 pp.

Prather, B.E., **O'Byrne, C.**, **Pirmez, C.** and **Sylvester, Z.** (2016) Sediment partitioning, continental slopes and base-of-slope systems. *Basin Res.*, 1–23.

Prélat, a., **Hodgson, D.M.** and **Flint, S.S.** (2009) Evolution, architecture and hierarchy of distributary deep-water deposits: a high-resolution outcrop investigation from the Permian Karoo Basin, South Africa. *Sedimentology*, **56**, 2132–2154.

Prélat, A., **Covault, J.A.**, **Hodgson, D.M.**, **Fildani, A.** and **Flint, S.S.** (2010) Intrinsic controls on the range of volumes, morphologies, and dimensions of submarine lobes. *Sediment. Geol.*, **232**, 66–76.

Reading, H.G. and **Richards, M.** (1994) Turbidite systems in deep-water basin margins classified by grain size and feeder system. *Am. Assoc. Pet. Geol. Bull.*, **78**, 792–822.

Richards, M., **Bowman, M.** and **Reading, H.** (1998) Submarine-fan systems I: characterization and stratigraphic prediction. *Mar. Pet. Geol.*, **15**, 689–717.

Romans, B.W., **Castelltort, S.**, **Covault, J.A.**, **Fildani, A.** and **Walsh, J.P.** (2016) Environmental signal propagation in sedimentary systems across timescales. *Earth-Science Rev.*, **153**, 7–29.

Romans, B.W., **Fildani, A.**, **Hubbard, S.M.**, **Covault, J.A.**, **Fosdick, J.C.** and **Graham, S.A.** (2011) Evolution of deep-water stratigraphic architecture, Magallanes Basin, Chile. *Mar. Pet. Geol.*, **28**, 612–628.

Salles, T., **Lopez, S.**, **Eschard, R.**, **Mulder, T.**, **Euzen, T.** and **Cacas, M.-C.** (2009) A turbidity-current model to simulate impact of basin-scale forcing parameters. *Extern. Control. Deep. Depos. Syst.*, **92**, 363–383.

Samuel, A., **Kneller, B.**, **Raslan, S.**, **Sharp, A.** and **Parsons, C.** (2003) Prolific deep-marine slope channels of the Nile Delta, Egypt. *Am. Assoc. Pet. Geol. Bull.*, **87**, 541–560.

Sequeiros, O.E. (2012) Estimating turbidity current conditions from channel morphology: A Froude number approach. *J. Geophys. Res.*, **117**, C04003.

Sequeiros, O.E., **Mosquera, R.** and **Pedocchi, F.** (2018) Internal Structure of a Self-Accelerating Turbidity Current. *J. Geophys. Res. Ocean.*, **123**, 6260–6276.

Sequeiros, O.E., **Spinewine, B.**, **Beaubouef, R.T.**, **Sun, T.**, **García, M.H.** and **Parker, G.** (2010a) Characteristics of Velocity and Excess Density Profiles of Saline Underflows and Turbidity Currents Flowing over a Mobile Bed. *J. Hydraul. Eng.*, **136**, 412–433.

Sequeiros, O.E., **Spinewine, B.**, **Beaubouef, R.T.**, **Sun, T.**, **García, M.H.** and **Parker, G.** (2010b) Characteristics of Velocity and Excess Density Profiles of Saline Underflows and Turbidity Currents Flowing over a Mobile Bed. *J. Hydraul. Eng.*, **136**, 412–433.

Sharma, S., **Bhattacharya, J.P.** and **Richards, B.** (2017) SOURCE-TO-SINK SEDIMENT BUDGET ANALYSIS OF THE CRETACEOUS FERRON SANDSTONE , UTAH , U . S . A ., USING THE FULCRUM APPROACH. 594–608.

Shumaker, L.E., **Jobe, Z.R.** and **Graham, S.A.** (2017) Evolution of submarine gullies on a prograding slope: Insights from 3D seismic reflection data. *Mar. Geol.*, **393**, 35–46.

Simmons, S.M., **Azpiroz-Zabala, M.**, **Cartigny, M.J.B.**, **Clare, M.A.**, **Cooper, C.**, **Parsons, D.R.**, **Pope,**

E.L., **Sumner, E.J.** and **Talling, P.J.** (2020) Novel acoustic method provides first detailed measurements of sediment concentration structure within submarine turbidity currents. *J. Geophys. Res. Ocean.*, e2019JC015904.

Somme, T.O., **Helland-hansen, W.**, **Martinsen, O.J.** and **Thurmond, J.B.** (2009a) Relationships between morphological and sedimentological parameters in source-to-sink systems: A basis for predicting semi-quantitative characteristics in subsurface systems. *Basin Res.*, **21**, 361–387.

Somme, T.O., **Martinsen, O.J.** and **Thurmond, J.B.** (2009b) Reconstructing morphological and depositional characteristics in subsurface sedimentary systems: An example from the maastrichtian-danian Ormen Lange system, M??re Basin, Norwegian Sea. *Am. Assoc. Pet. Geol. Bull.*, **93**, 1347–1377.

Somme, T.O., **Piper, D.J.W.**, **Deptuck, M.E.** and **Helland-Hansen, W.** (2011) Linking Onshore-Offshore Sediment Dispersal in the Golo Source-to-Sink System (Corsica, France) During the Late Quaternary. *J. Sediment. Res.*, **81**, 118–137.

Somme, T.O., and Martinsen, O.J. (2017) *Deep-water depositional systems conference*, The Geological Society, London, 25-27th January 2017**.**

Stacey, C.D., **Hill, P.R.**, **Talling, P.J.**, **Enkin, R.J.**, **Hughes Clarke, J.** and **Lintern, D.G.** (2019) How turbidity current frequency and character varies down a fjord-delta system: Combining direct monitoring, deposits and seismic data. *Sedimentology*, **66**, 1–31.

Stacey, M.W. and **Bowen, A.J.** (1988) The vertical structure of density and turbidity currents: Theory and observations. *J. Geophys. Res.*, **93**, 3528–3542.

Stevens, T., **Paull, C.K.**, **Ussler, W.**, **McGann, M.**, **Buylaert, J.P.** and **Lundsten, E.** (2014) The timing of sediment transport down Monterey Submarine Canyon, offshore California. *Bull. Geol. Soc. Am.*, **126**, 103–121.

Stevenson, C.J., **Feldens, P.**, **Georgiopoulou, A.**, **Schönke, M.**, **Krastel, S.**, **Piper, D.J.W.**, **Lindhorst, K.** and **Mosher, D.** (2018) Reconstructing the sediment concentration of a giant submarine gravity flow. *Nat. Commun.*, **9**, 1–7.

Stevenson, C.J., **Jackson, C.A.-L.**, **Hodgson, D.M.**, **Hubbard, S.M.** and **Eggenhuisen, J.T.** (2015a) Deep-water sediment bypass. J Sediment Res. doi: 10.2110/jsr.2015.63

Straub, K.M. and **Mohrig, D.** (2008) Quantifying the morphology and growth of levees in aggrading submarine channels. *J. Geophys. Res. Earth Surf.*, **113**, 1–20.

Straub, K.M., **Mohrig, D.**, **McElroy, B.**, **Buttles, J.** and **Pirmez, C.** (2008) Interactions between turbidity currents and topography in aggrading sinuous submarine channels: A laboratory study. *Geol. Soc. Am. Bull.*, **120**, 368–385.

Strong, N. and **Paola, C.** (2008) Valleys that never were: Time surfaces versus stratigraphic surfaces. *J. Sediment. Res.*, **78**, 579–593.

Syvitsky, J.P.M. and **Milliman, J.D.** (2007) Geology , Geography , and Humans Battle for Dominance over the Delivery of Fluvial Sediment to the Coastal Ocean. *J. Geol.*, **115**, 1–19.

Talling, P.J., **Masson, D.G.**, **Sumner, E.J.** and **Malgesini, G.** (2012) Subaqueous sediment density flows: Depositional processes and deposit types. *Sedimentology*, **59**, 1937–2003.

Talling, P.J., **Paull, C.K.** and **Piper, D.J.W.** (2013) How are subaqueous sediment density flows triggered, what is their internal structure and how does it evolve? Direct observations from monitoring of active flows. *Earth-Science Rev.*, **125**, 244–287.

Tilston, M., Arnott, R.W.C., Rennie, C.D. and **Long, B. (2015)** The influence of grain size on the velocity and sediment concentration profiles and depositional record of turbidity currents. *Geology*, **43**, 839–842.

Traer, M.M., **Hilley, G.E.**, **Fildani, A.** and **McHargue, T.** (2012) The sensitivity of turbidity currents to mass and momentum exchanges between these underflows and their surroundings. *J. Geophys. Res. Earth Surf.*, **117**, n/a-n/a.

Van Rijn, L.C. (2011) Principles of fluid flow and surface waves in rivers, estuaries, seas, and oceans., 2011th edn. *Aqua Publications*.

Walsh, J.P., **Wiberg, P.L.**, **Aalto, R.** and **Kuehl, S.A.** (2016) Source-to-sink research: economy of the Earth’s surface and its strata. *Earth Sci. Rev.*, **153**, 1–6.

Wang, Z., Xu, J., Talling, P.J., Cartigny, M.J.B., Simmons, S.M., Gwiazda, R., Paull, C.K., Maier, K.L. and Parsons, D.R. (2020) Direct evidence of a high-concentration basal layer in a submarine turbidity current. *Deep. Res. Part I Oceanogr. Res. Pap.*, **161**, 103300.

Xu, J.., **Noble, M.**, **Eittreim, S.L.**, **Rosenfeld, L.K.**, **Schwing, F.B.** and **Pilskaln, C.H.** (2002) Distribution and transport of suspended particulate matter in Monterey Canyon, California. *Mar. Geol.*, **181**, 215–234.

Xu, J.P. (2011) Measuring currents in submarine canyons: Technological and scientific progress in the past 30 years. *Geosphere*, **7**, 868–876.

Xu, J.P., **Noble, M.A.** and **Rosenfeld, L.K.** (2004) In-situ measurements of velocity structure within turbidity currents. *Geophys. Res. Lett.*, **31**, 1–4.

Zeng, J., **Lowe, D.R.**, **Prior, D.B.**, **Wiseman, W.J.** and **Bornhold, B.D.** (1991) Flow properties of turbidity currents in Bute Ilte, British Columbia. *Sedimentology*, **38**, 975–996.